ZIRCONOLITE AND Zr–Th–U MINERALS IN CHROMITITES OF THE FINERO COMPLEX, WESTERN ALPS, ITALY: EVIDENCE FOR CARBONATITE-TYPE METASOMATISM IN A SUBCONTINENTAL MANTLE PLUME

Federica ZACCARINI§ and Eugen F. STUMPFL†

Department of Applied Geological Sciences and Geophysics, University of Leoben,
Peter Tunner Str. 5, A–8700 Leoben, Austria

Giorgio GARUTI

Dipartimento di Scienze della Terra, Università di Modena e Reggio Emilia, Via S.Eufemia, 19, I–41100 Modena, Italy

Abstract

Zirconolite ($CaZrTi_2O_7$) associated with baddeleyite (ZrO_2), thorianite (ThO_2), uraninite (UO_2), thorite or huttonite ($ThSiO_4$) and zircon ($ZrSiO_4$) has been discovered in chromitites of the Finero mantle-derived massif, in the Western Alps of Italy. The "exotic" minerals do not occur in late veins or fractures; they are part of the accessory assemblage (phlogopite, amphibole, apatite, ilmenite, geikielite, rutile, molybdenite, and Mg–Ca carbonates) formed as a result of metasomatism of the Finero mantle. Textural relations of zirconolite and the Zr–Th–U minerals indicate crystallization with the chromite – olivine – orthopyroxene assemblage between 800° and ~600°C, at a given pressure of 1.0 GPa. Zirconolite is an indicator of silica-undersaturated conditions. Its composition, characterized by the prevalence of Th and U over Nb and Ta, is similar to that of zirconolite from some carbonatite complexes. The close association with Zr–Th–U minerals, and with the carbonatite-compatible elements Y, Hf, Pb, and LREE, is symptomatic of the carbonatitic character of metasomatism at Finero. The formation of a carbonatite-type liquid and related hydrous fluid is commonly related to the emplacement of mantle plumes in continental rift systems worldwide. This supports the inference that the metasomatism of the Finero mantle was a result of mantle diapirism at the base of the continental crust induced by extensional tectonics in pre-Hercynian times.

Keywords: zirconolite, baddeleyite, thorianite, uraninite, thorite or huttonite, zircon, chromitite, carbonatite metasomatism, Finero Complex, Western Alps, Italy.

Sommaire

Nous avons trouvé la zirconolite ($CaZrTi_2O_7$) associée aux accessoires baddeleyite (ZrO_2), thorianite (ThO_2), uraninite (UO_2), thorite ou huttonite ($ThSiO_4$) et zircon ($ZrSiO_4$) dans des échantillons de chromitite du massif de Finero, de dérivation mantellique, dans les Alpes occidentales, en Italie. Ces minéraux "exotiques" ne se présentent pas en veines ou fractures tardives; ils font bien partie de l'assemblage des accessoires (phlogopite, amphibole, apatite, ilménite, geikielite, rutile, molybdénite, et carbonate de Mg–Ca) formée lors d'une métasomatose dans le manteau. Les relations texturales de la zirconolite et des minéraux à Zr–Th–U associés indiquent une cristallisation avec l'assemblage chromite – olivine – orthopyroxène entre 800° et environ 600°C, à une pression d'environ 1.0 GPa. La zirconolite est un indicateur de sous-saturation en silice. Sa composition dans cet suite, par exemple la pro-éminence de Th et U par rapport à Nb et Ta, rappelle la zirconolite signalée dans certains complexes carbonatitiques. Son étroite association aux minéraux de Zr–Th–U et aux éléments Y, Hf, Pb et terres rares légères, serait symptomatique d'un caractère carbonatitique de la métasomatose qui a affectée ce complexe. La formation d'un liquide d'aspect carbonatitique et d'une phase fluide associée est généralement liée à la mise en place de panaches mantelliques dans les rifts continentaux. Cette association concorde donc avec l'hypothèse voulant que le manteau à Finero ait subi un diapirisme à la base de la croûte continentale au cours d'un épisode pré-Hercynien de tectonique d'extension.

(Traduit par la Rédaction)

Mots-clés: zirconolite, baddeleyite, thorianite, uraninite, thorite ou huttonite, zircon, chromitite, métasomatose carbonatitique, complexe de Finero, Alpes occidentales, Italie.

§ *E-mail address*: fedezac@tsc4.com
† Deceased July 12, 2004.

INTRODUCTION

Zirconolite (ideally: $CaZrTi_2O_7$) is a rare oxide mineral; it has so far been reported from a few terrestrial localities, lunar basalts and meteorites (Busche *et al.* 1972, Sheng *et al.* 1991, Williams & Gieré 1996, Gieré *et al.* 1998). Despite of its relative scarcity in terrestrial rocks, zirconolite occurs in a variety of lithological associations, mainly silica-undersaturated alkaline rocks, such as carbonatite, phoscorite, syenite, nepheline syenite, potassic lavas (Mazzi & Munno 1983, Fowler & Williams 1986, Platt *et al.* 1987, Bulakh *et al.* 1998, 1999, Bellatreccia *et al.* 1999, De Hoog & Van Bergen 2000, Della Ventura *et al.* 2000), and metasomatized carbonate rocks (skarns) at the contact with intrusive bodies (Gieré 1986, Purtscheller & Tessadri 1985, Zakrzewski *et al.* 1992). It also occurs in metarodingites (Stucki *et al.* 2001) and, sporadically, in mafic–ultramafic rocks of layered intrusions (Williams 1978, Harding *et al.* 1982, Lorand & Cottin 1987, Sonnenthal 1992), and metasomatized ophiolitic chromitites (Proenza *et al.* 2001). Zirconolite has further been found in mantle xenoliths (Haggerty 1987, Horning & Wörner 1991) and lamproites (Carlier & Lorand 2003). In a recent review of the mineralogy of the upper mantle, as illustrated by xenoliths associated with alkali basalts and kimberlites (Haggerty 1995), zirconolite has been included in the group of rare and "exotic" mineral oxides, carriers of large-ion lithophile elements (LILE) and high field-strength elements (HFSE) that may form in the mantle as a result of fluid-driven metasomatic processes.

In this paper, we report the first documented occurrence of zirconolite and other Zr–Th–U minerals (zircon, baddeleyite, thorianite, uraninite, thorite or huttonite) in podiform chromitites of the phlogopite peridotite massif of Finero, in the Ivrea Zone, Western Alps, Italy. The Finero massif represents an important example of partially depleted upper mantle, re-enriched by reaction with flushing alkaline fluids carrying incompatible elements and volatiles. Secondary PKP (phlogopite – K-bearing richterite peridotite) and MARID (mica – amphibole – rutile – ilmenite – diopside) assemblages typical of metasomatized mantle xenoliths (Erlank *et al.* 1987, Harte *et al.* 1987, Dawson & Smith 1977) are associated with a strongly residual assemblage (olivine – orthopyroxene – chromian spinel) in a fresh and coarse-grained recrystallized harzburgite. Various aspects of metasomatism at Finero are currently subject to discussion and debate. For example, the questions of the provenance (mantle or crust) of the metasomatic fluids (Ernst 1981, Exley *et al.* 1982), and the geodynamic environment, either a subcontinental mantle plume (Shervais & Mukasa 1991, Garuti *et al.* 2001) or a subduction setting (Hartmann & Wedepohl 1993, Zanetti *et al.* 1999, Morishita *et al.* 2003) remain unresolved. The discovery of zirconolite and accessory Zr–Th–U minerals in the Finero chromitites provides new insights into the composition of the metasomatic fluids and raises new questions concerning the geological setting of the mantle massifs of the Ivrea Zone.

GEOLOGICAL SETTING AND FIELD RELATIONS

The Ivrea Zone of the Western Alps (Fig. 1A) represents a tilted block of lower continental crust, consisting of mafic and ultramafic layered rocks (the Basic Complex) intruded into granulite- to amphibolite-facies metasedimentary and metavolcanic rocks of the Kinzigite Series. The Finero phlogopite peridotite is the largest of three mantle massifs exposed at the base of the lower crust in this area. It forms the core of a roughly elliptical, antiformal structure consisting of a concentrically zoned sequence of layered amphibole-rich, garnet-bearing gabbro and pyroxenite, amphibole-rich peridotite, and gabbro, passing outward into granulite-facies metasedimentary units (Fig. 1B). Details of the geology and petrography are given by Lensch (1968), Cawthorn (1975), Ernst (1978) and Coltorti & Siena (1984). The Finero massif is chemically distinct from the other mantle-derived massifs of the Ivrea Zone. It consists of "flushed" harzburgite, characterized by a residual assemblage (olivine, orthopyroxene, chromian spinel) attributed to extraction of about 18% MORB-like melt. Metasomatic re-enrichment has its mineralogical expression in the extensive crystallization of phlogopite, amphibole, apatite, and carbonates; geochemically, it is characterized by abnormal re-enrichment in Rb, Ba, K, Pb, Sr, the light rare-earth elements (LREE), Na and Au (Exley *et al.* 1982, Stähle *et al.* 1990, Hartmann & Wedepohl 1993, Garuti *et al.* 1997, Morishita *et al.* 2003). Mantle metasomatism was initiated 293 ± 13 Ma ago (Cummings *et al.* 1987, Voshage *et al.* 1987) by reaction of the depleted protolith with an alkaline, volatile-rich fluid phase that, according with some authors, may have been derived from a crustal slab in a subduction setting (Hartmann & Wedepohl 1993, Zanetti *et al.* 1999, Morishita *et al.* 2003). An alternative interpretation is that the Finero phlogopite peridotite, together with the other lherzolite massifs of the Ivrea Zone, Balmuccia and Baldissero (Fig. 1), may represent variously depleted and re-enriched parts of a mantle plume emplaced at the base of the subcontinental crust by extension and thinning of the lithosphere, in pre-Hercynian times (Exley *et al.* 1982, Stähle *et al.* 1990, Shervais & Mukasa 1991, Henk *et al.* 1997, Garuti *et al.* 2001). Similarities in age, trace-element and Sr–Nd–S isotope geochemistry indicate that metasomatism of the Finero mantle possibly was linked to the intrusion of alkaline ultramafic magmas that characterized the closure of underplating in the Ivrea Zone, at about 287 ± 3 Ma (Garuti *et al.* 2001). Crystallization of phlogopite at 220–206 Ma marks the main stage of metasomatism at about 800°C (Hunziker 1974), and is accompanied by partial recrystallization of olivine, which reveals a dominant α-fabric almost at right angle to the mica foliation (Garuti & Friolo 1978).
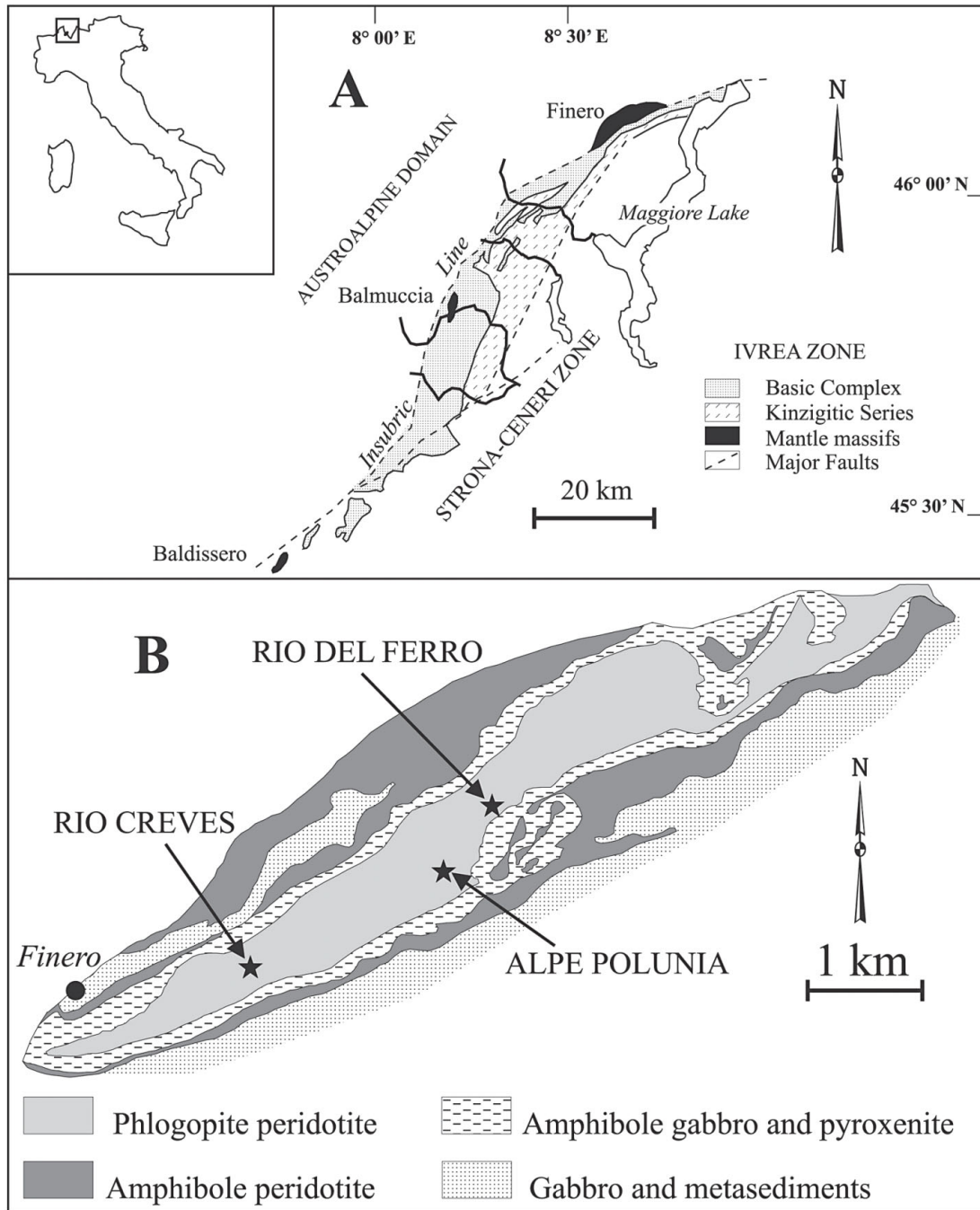
FIG. 1.   Simplified geological map of A) the Ivrea–Verbano zone showing the location of the Finero, Balmuccia and Baldissero mantle-derived massifs, and B) the Finero complex, showing location of the occurrences of chromitite investigated (black stars).

An age of 208 ± 2 Ma for zircon associated with chromitite at Rio Creves has been proposed (Von Quadt *et al.* 1993, Grieco *et al.* 2001).

Small bodies of chromitite occur at various localities in the phlogopite peridotite of Finero (Ferrario & Garuti 1990). The chromitites have morphological characteristics similar to podiform chromitites from the mantle tectonite of ophiolites, although the orebodies are distinctly smaller, and the effects of low-P, low-T oceanic metamorphism, typical of ophiolites, are lacking. The geometry and relationships with the host rocks are well exposed in old exploration workings near Alpe Polunia and Rio Creves (Fig. 1B). Here, a chromitite horizon has been traced discontinuously over some hundred meters, along the southern border of the phlogopite peridotite unit. The chromitite forms distinct layers and elongate lenses, up to one meter long and a few tens of centimeters thick, in coarse-grained harzburgite and dunite. Some orebodies have the typical "schlieren" morphology, with repetitive millimetric to centrimetric seams of chromitite over a lateral distance of 5–50 centimeters. More extensive layers and lenses are symmetrically zoned and consist of an internal core of coarse-grained spinel (up to 1 cm across) intergrown with 20 to 50 vol.% silicate matrix (mainly orthopyroxene and olivine), with margins of alternating bands of fine-grained spinel and silicates. The contacts with the enclosing dunite are generally sharp and marked by a zone of orthopyroxene enrichment.

Ferrario & Garuti (1990) suggested that the chromitites formed concomitantly with the episode of alkaline metasomatism. A reaction seems to have taken place between the residual mantle and the metasomatic fluid phase causing instability of chromian diopside and the crystallization of abundant Ti-rich chromite associated with Ti-rich enstatite and pargasite, phlogopite, and olivine, now occurring as inclusions in chromite. Although this model may no longer account for all observations and data, the presence of abundant phlogopite, zircon, molybdenite and Mg-carbonates as part of the accessory assemblage of the chromitites reflects beyond any doubt a reaction with flushing fluids enriched in incompatible elements.

SAMPLING AND ANALYTICAL METHODS

Zirconolite and the Zr–Th–U minerals were discovered in chromitite samples collected from the dump in the prospecting trenches of Alpe Polunia and Rio Creves, and from an erratic boulder of chromitite in Rio del Ferro. The grains were initially located by scanning the polished sections at approximately ×100 magnification with a Philips XL40 scanning electron microscope (SEM) operated in back-scattered electron (BSE) mode, at an accelerating voltage of 20–30 kV and a beam current of 2–10 nA. Morphological and textural details of the grains were investigated at a higher magnification, as reported in the BSE images presented in this work. The qualitative composition of the grains was initially determined using energy-dispersion spectrometry (EDS) on the SEM instrument. Subsequently, quantitative analysis was performed in wavelength-dispersion mode using an ARL–SEMQ electron microprobe operated at an excitation voltage of 15–20 kV and a beam current of 15 nA, with a beam diameter of about 1 μm. Owing to the small size of the grains (usually <10 μm), and because of the contemporaneous presence of elements (*i.e.*, Ca, Ti, Fe, Mg) in the analyzed grains as well as in the adjacent phases, optimum counting-times as short as 20 and 5 seconds for peak and background, respectively, were experimentally determined to minimize spurious fluorescence from the matrix. Natural chromite, olivine, clinopyroxene, ilmenite, garnet, biotite, albite and microcline were used as standards for Cr, Fe, Mg, Ca, Ti, Al, Na and K. The elements Ba, Sr, P, Zr, Hf, Y, U, Th, Pb and the REE (La, Ce, Pr, Nd) were calibrated on natural barite, celestine, apatite, monazite, crocoite, and on the synthetic compounds ThO_2, ZrO_2, $UCoSi$, La_2YSi_2, Ce_2YSi_2, NdSi, PrSi, and metallic Hf. Fluorine and Cl were standardized on fluorite and tugtupite ($Na_4BeAlSi_4O_{12}Cl$, containing 7.58 wt% Cl). On-line reduction of data and automatic correction of the observed interference between various pairs of elements were performed with version 3.63 of the PROBE software, updated January 1996 (Donovan & Rivers 1990). The detection limits for the trace elements sought are reported in the tables. The proportion of Fe^{3+} in spinel phases was calculated assuming the stoichiometry $R^{2+}O\ R^{3+}_2O_3$.

PETROGRAPHY OF THE SAMPLES

The chromitite samples containing the Zr–Th–U minerals are composed of 80 to 20 vol.% chromian spinel and are dominated by the reaction textures described by Ferrario & Garuti (1990). Massive chromitite consists of relatively coarse-grained (up to 2–3 mm) chromian spinel, characterized by rounded and lobate boundaries with the silicates, commonly with amoeboid intergrowths and reciprocal inclusions, a texture suggestive of the contemporaneous nucleation of oxides and silicates (Figs. 2A, B, C). A second type of spinel is observed in the reaction textures. It is characterized by lower reflectance and higher transparency (with a light brown to dark green color) compared with the groundmass chromian spinel. Generally it forms drop-like, vermicular or symplectitic intergrowths inside olivine, in some cases associated with amphibole, typically developed along the contacts between the massive chromian spinel and the silicate (Figs. 2D, E, F). These features may indicate spinel exsolution from the silicate, or precipitation of spinel by reaction between silicates and chromian spinel induced by fluids or, considered less likely, infiltration of a spinel-crystallizing melt along contacts, crystallographic planes and cleavages of the silicate.

The coarse-grained chromian spinel has Cr# [Cr/(Cr + Al) atomic ratio] and Fe^{2+}# [Fe^{2+}/(Fe^{2+} + Mg) atomic ratio] in the ranges 0.60–0.70 and 0.35–0.50, respectively. It is thus ferroan magnesiochromite. The varia-

tion in Fe^{2+}# is mainly controlled by variation in the mass ratio of chromian spinel to silicate, with the more disseminated grains of spinel (<30% by volume) being shifted toward Fe-rich and Mg-poor compositions.
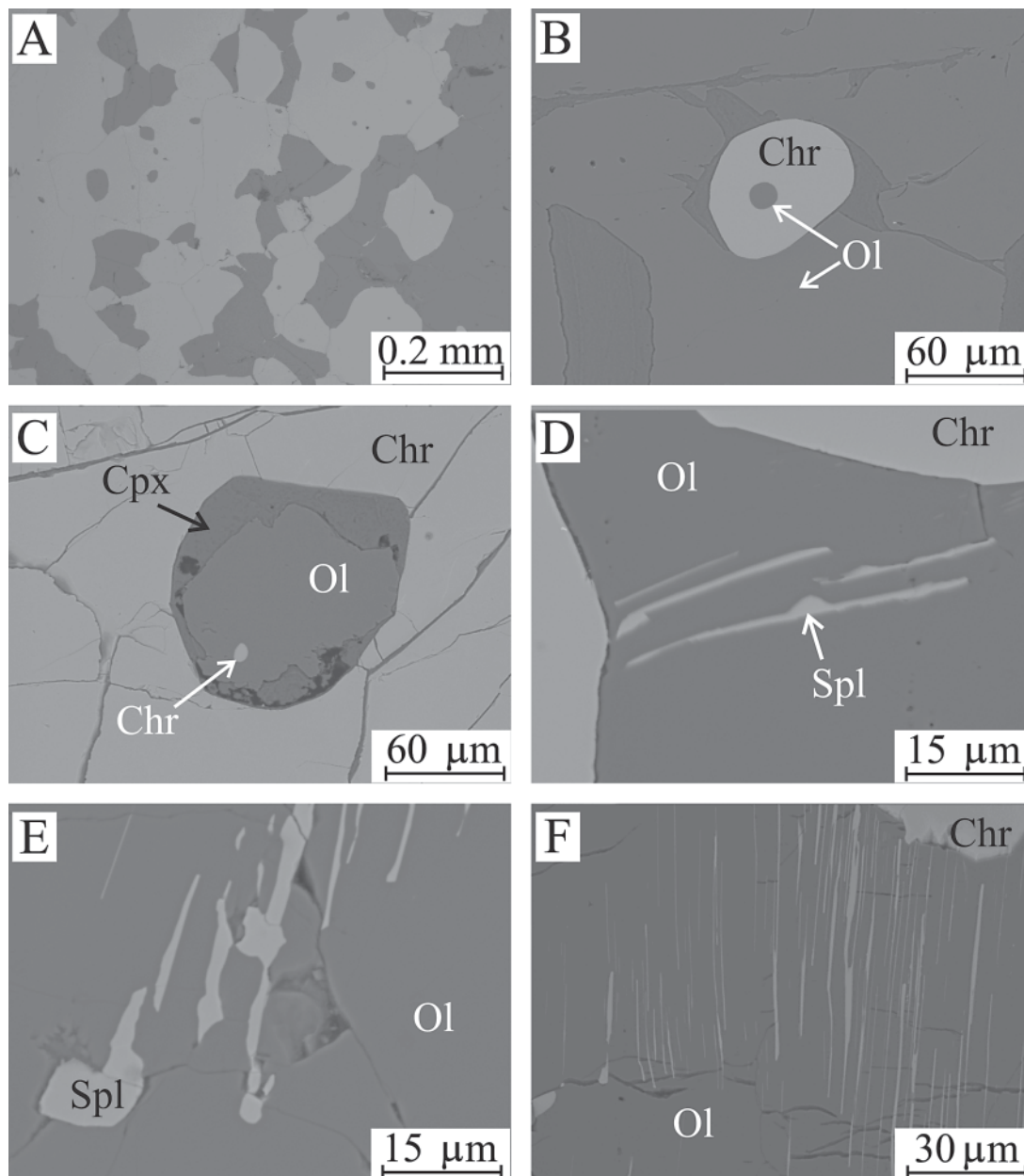
FIG. 2.   Textural relations of spinel in the chromitite of Finero (BSE images). A) Massive chromian spinel (light grey) with rounded and lobate boundaries with silicates (dark grey). B, C) Reciprocal inclusions of olivine and chromian spinel. In C, olivine is partially replaced by clinopyroxene. D,E,F) Symplectitic intergrowths of spinel and olivine. Symbols: Chr: massive chromian spinel, Spl: Fe–Al spinel, Ol: olivine, Cpx: clinopyroxene.

Weak core-to-rim compositional zoning has been observed, with the rim enriched in Fe and depleted in Cr or *vice versa*. The TiO_2 content varies from 0.45 to 0.84 wt%, and the content of Fe_2O_3, from 4.4 to 9.6 wt%. Spinel grains from symplectites are variably enriched in total Fe and Al, and have lower Cr compared with the coexisting massive chromian spinel. They also have high Zn and V contents and low concentrations of Ti, especially where in contact with Ti-oxides. Mg-rich ilmenite (2.7–9.89 wt%), geikielite (15 wt% MgO) and rutile are encountered as part of the symplectite asemblage, occurring as either small drop-like grains or large patches associated with the (Al,Fe)-rich spinel.

The major constituents of the silicate matrix are olivine, orthopyroxene, clinopyroxene and amphibole, in decreasing order of abundance. They have lower $Fe^{2+}\#$ compared to analogous minerals in the massive phlogopite peridotite reported by Coltorti & Siena (1984). The forsterite content of olivine increases from 90–93% to 93–97% Fo, in olivine from silicate-rich bands, to olivine interstitial to or included in massive chromian spinel, respectively. The Ni content increases in parallel with Mg/Fe, and reaches values as high as 0.75 wt% NiO in olivine inclusions. Orthopyroxene contains 93–94 mol.% enstatite and is depleted in Cr and enriched in Al with respect to orthopyroxene from the peridotite groundmass. Clinopyroxene contains less than 1.25 wt% Al_2O_3, up to 1.98 wt% FeO, 0.23 wt% TiO_2, 0.45 wt% Na_2O and 0.55 wt% Cr_2O_3. Amphibole is enriched in Na (3.68 wt% Na_2O), Ti (2.21 wt% TiO_2) and Cr (2.35 wt% Cr_2O_3).

The chromitites also contain a suite of accessory minerals, phlogopite, apatite and Ca–Mg carbonates, interpreted to be the result of metasomatism (Ferrario & Garuti 1990). Phlogopite is a common constituent of inclusions incorporated in the massive chromian spinel, generally associated with clinopyroxene, sulfides (mainly chalcopyrite, bornite, and millerite), and native copper (Figs. 3A, B). Carbonates mostly occur as part of composite inclusions (carbonate + silicate + sulfide)
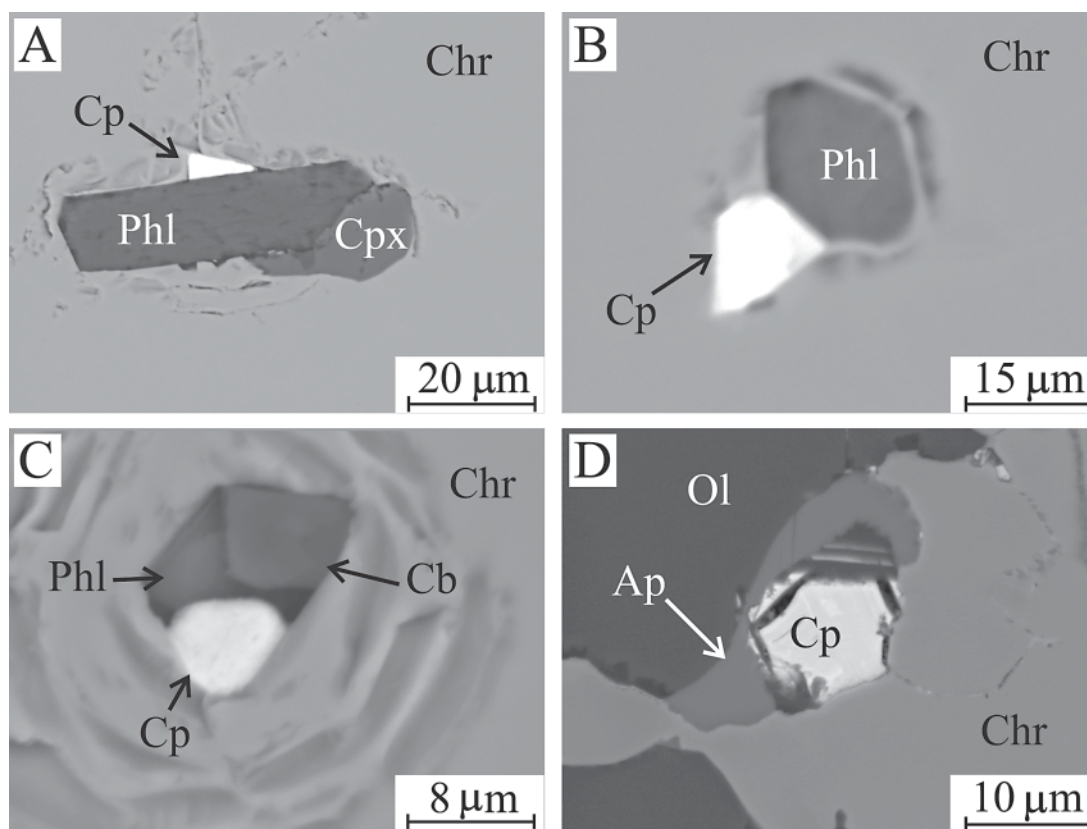
FIG. 3. Accessory metasomatic minerals in the Finero chromitite (BSE images). A) Polyphase inclusion of phlogopite, clinopyroxene and chalcopyrite in massive chromian spinel. B) Phlogopite and chalcopyrite included in massive chromian spinel. C) Polyphase inclusion of phlogopite, chalcopyrite and Ca–Mg carbonate in massive chromian spinel. D) Apatite and chalcopyrite at the contact between massive chromian spinel and olivine. Symbols: Phl: phlogopite, Cp: chalcopyrite, Cb: Ca–Mg carbonate, Ap: apatite; see Figure 2 for other symbols.

in the massive chromian spinel (Fig. 3C), but have also been observed in the silicate matrix. Apatite (maximum grain-size 100 μm) is quite common. Usually, it occurs either associated with (but never included in) the chromian spinel (Fig. 3D) or as part of the vermicular-spinel symplectite assemblage along with zirconolite and baddeleyite, its texture indicating cocrystallization with the oxides (see below).

ZIRCONOLITE AND THE ZR–TH–U MINERALS

Distribution and paragenetic assemblage

Zirconolite in the chromitites of Finero is usually accompanied by baddeleyite (ZrO_2), zircon ($ZrSiO_4$), members of the thorianite–uraninite series [$(Th,U)O_2$], and a silicate of thorium, either thorite or huttonite ($ThSiO_4$). Only zircon had previously been reported (Ferrario & Garuti 1990), probably owing to its considerably larger grain-size (up to 300 μm) compared with the other components of the assemblage, which rarely exceed 20 μm and are commonly less than 10 μm. Therefore, we report here the first documented occurrence of these Zr–Th–U minerals in the Finero complex.

More than sixty grains were encountered in seven polished sections, with an average frequency of about three grains per square centimeter. Identification by optical microscopy was hampered by their extremely small grain-size and low reflectance. Scanning electron microscopy thus facilitated their identification. The very small size of the grains also prevented determination of structural data; therefore, attribution to the various mineral species had to be based solely on determination of chemical composition and stoichiometry obtained by electron-microprobe analysis. The relative proportion of Zr–Th–U minerals, expressed as number of grains, indicates a predominance of zirconolite and baddeleyite over the other phases. Morphology, mode of occurrence and paragenetic association of the Zr–Th–U accessory minerals are illustrated in a series of BSE images (Figs. 4 to 6).

Zirconolite was found in five samples of chromitite from the old exploration trenches of Alpe Polunia and Rio Creves. The mineral occurs as small crystals ranging in size from 3 to 20 μm. At high magnification, most grains seem to have a consistent polygonal shape. Zirconolite may occur as isolated grains in olivine of the silicate matrix, although it typically occurs associated with minute drops of and in symplectitic intergrowth with (Fe,Al)-rich spinel within olivine (Fig. 4). Conspicuously, it is never found included in massive chromian spinel. Zirconolite has also been found in contact or in close spatial association with ilmenite, rutile, geikielite and apatite (Figs. 4C, 5A, B, C), supporting a common origin of the assemblage. In some cases, zirconolite forms composite grains with baddeleyite. Some grains of zirconolite were found to have an irregular shape determined by an irregular grain-bound-ary (Fig. 5). Several minute (<1 μm) bright grains containing abundant Th and U are visible along the rim. The BSE images show that this type of zirconolite is in contact with partially altered spinel and thin cracks and fissures filled with serpentine. Thus, the formation of the Th–U mineral assemblage is interpreted as a result of alteration by reaction with hydrous fluids, at very low temperature.

Baddeleyite predominates in chromitite samples from Alpe Polunia. It forms polygonal crystals varying from 3 to 15 μm in size. Baddeleyite may occur closely intergrown with fine-grained spinel disseminated in the silicate matrix (Fig. 6A). However, a number of baddeleyite grains were found located at the boundary of coarse-grained chromian spinel in external contact with olivine, suggesting growth of the zirconium oxide on chromite (Fig. 6B). Some grains of baddeleyite are associated with amphibole and Fe–Al spinel (Fig. 6C).

Zircon was encountered in samples from Rio Creves, Alpe Polunia and Rio del Ferro. The mineral is relatively abundant and generally occurs as large crystals (50–200 μm) characterized by subhedral to euhedral shapes, usually in contact with or molded on the external boundary of the groundmass chromian spinel (Fig. 6D). More rarely, zircon appears to be totally included in the silicate matrix (Fig. 6E).

Thorianite and uraninite occur in chromitite samples from the exploration trench of Rio Creves. Most grains consist of subhedral to euhedral crystals, up to about 20 μm in size, either at the boundary of chromian spinel (Fig. 6F) or in close vicinity, inside orthopyroxene of the silicate matrix. In all cases, the grains of Th–U oxide are located far from fractures or serpentine veins, and do not display spatial relationships with other members of the Zr-rich assemblage (zirconolite, baddeleyite, zircon), or any of the other accessory phases such as Al–Fe spinel, ilmenite, rutile or apatite.

Thorite or huttonite occurs in chromitite samples from both Alpe Polunia and Rio Creves, generally as polygonal grains located in the silicate matrix, in some cases in contact with chromian spinel. The largest grain, about 15 μm across, was found at the contact between amphibole and orthopyroxene. Identification is based on electron-microprobe data only; the small grain-size prevented X-ray-diffraction analysis.

Composition of zirconolite

Zirconolite (Table 1) has the ideal formula $CaZrTi_2O_7$, in which the available cationic sites have 8-fold coordination (Ca), 7-fold coordination (Zr), and 5- and 6-fold coordination (Ti). The Finero zirconolite deviates from the theoretical composition because only the 7-fold coordinate site is almost fully occupied (by Zr); up to 35% of the Ca site and 15% of Ti site are occupied by other cations. Electron-microprobe analyses reveal substantial amounts of Th (8.52–13.77 wt% ThO_2) and U (1.4–4.75 wt% UO_2); one sample from Rio Creves

has 12.13 wt% UO_2. The contents of Fe (4.41–6.75 wt% FeO) and Mg (0.66–1.77 wt% MgO) are also relatively high compared to published ranges in natural zirconolite (Williams & Gieré 1996). The Finero zirconolite also contains rare-earth elements (0.57–1.69 wt% Nd_2O_3,

0.28–0.94 wt% Ce_2O_3, <0.35% La_2O_3), Y (0.29–0.66 wt% Y_2O_3), Hf (0.70 wt% HfO_2) and Si (0.11–1.43 wt% SiO_2), although concentrations are considerably lower than the maximum contents reported in the literature. Trace amounts of Pb (0.54 wt% PbO) have been de-
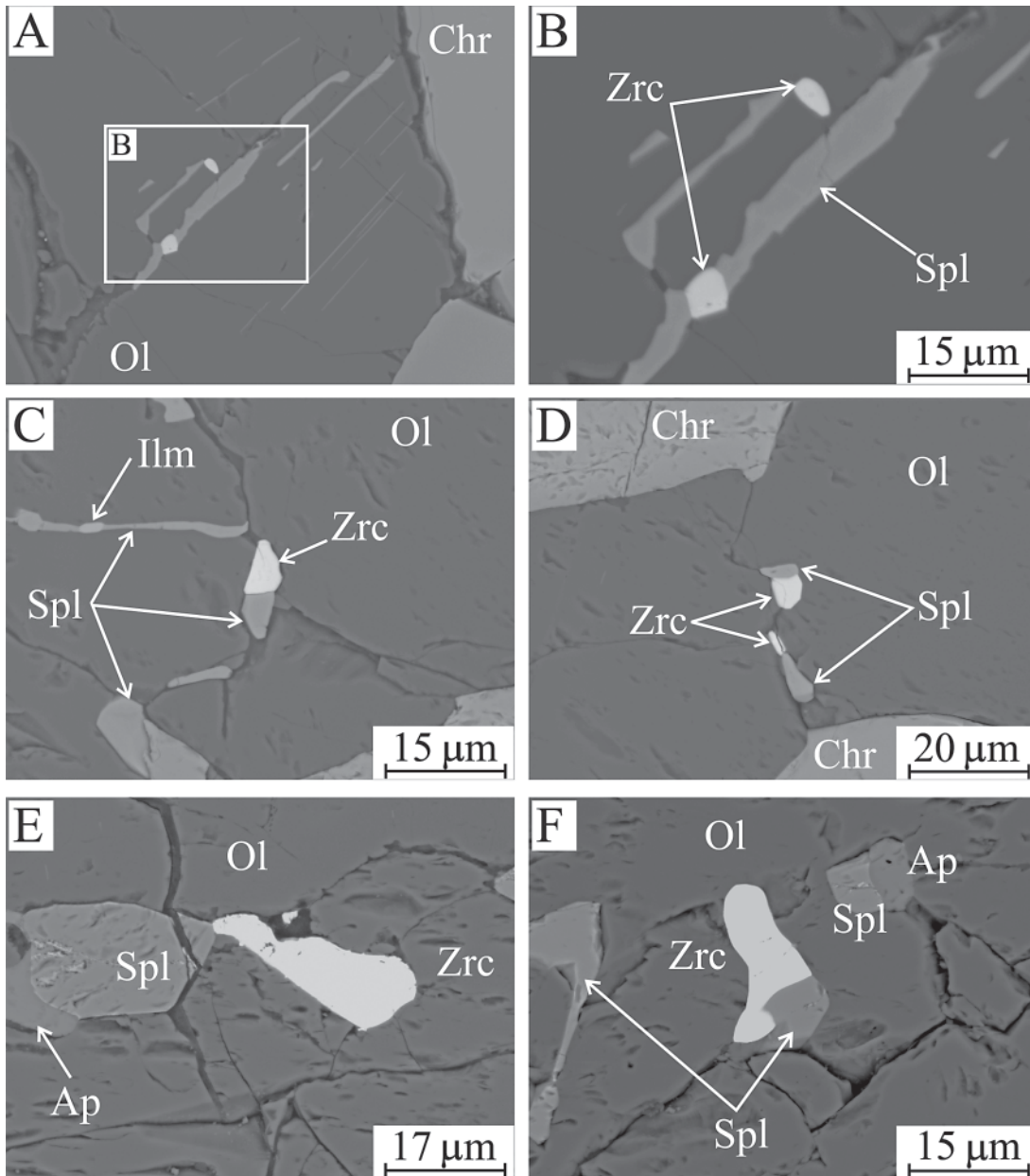

FIG. 4.   Textural relations of zirconolite in the Finero chromitite (BSE images). A, B) Zirconolite associated with spinel symplectite, in olivine. C, D) Zirconolite associated with spinel (and ilmenite) interstitial to olivine. E, F) Zirconolite associated with spinel and apatite, interstitial to olivine. Symbol: Zrc = zirconolite; see Figure 2 for other symbols.
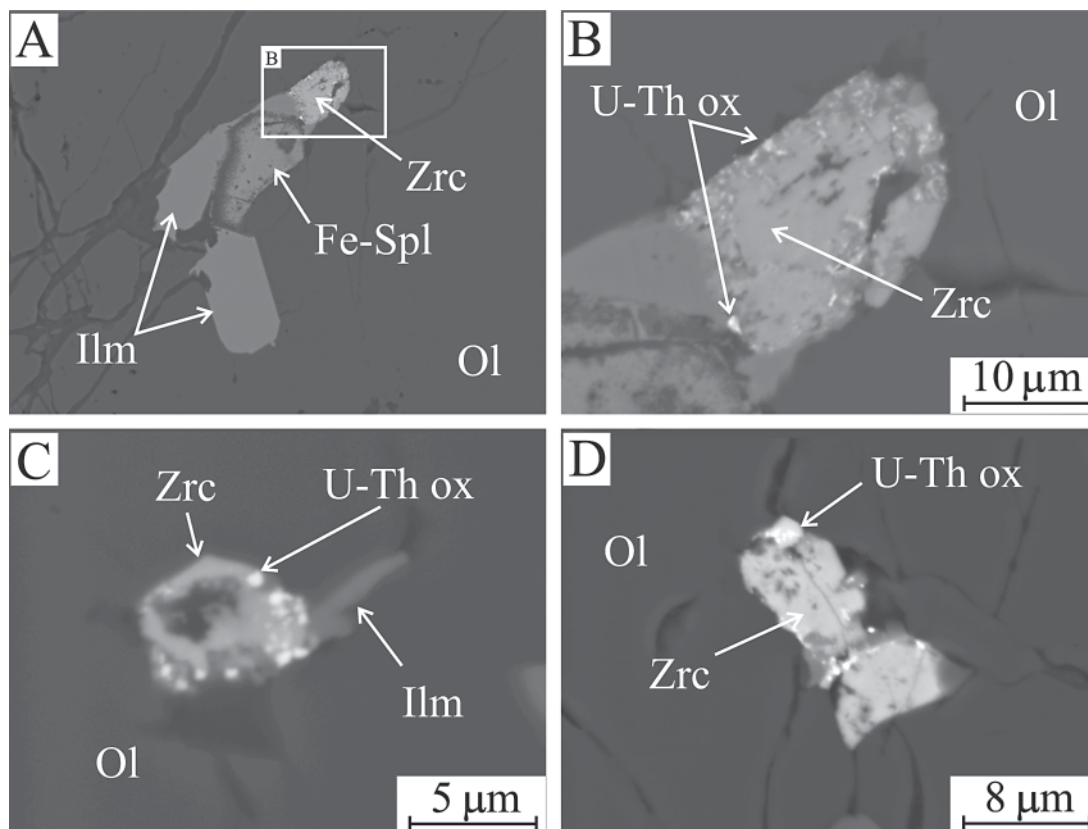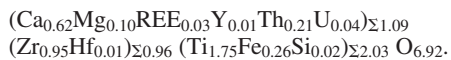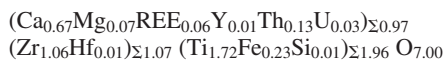
FIG. 5.   Textural relations of zirconolite in the Finero chromitite (BSE images). A) "Altered" zirconolite associated with ilmenite and ferrian chromite. B) Enlargement of A) showing minute particles of U and Th oxide along the boundary of the zirconolite grain. C, D) "Altered" zirconolite with U and Th oxides (white blebs) interstitial to olivine. Symbols: Ilm: ilmenite, Fe-Spl: ferrian chromite, U–Th ox: unidentified uranium–thorium oxide; see Figure 2 for other symbols.

amounts of Hf to the Zr site. Single grains were found to be compositionally homogeneous. However, small grain-to-grain variations were observed on the polished-section scale, mainly involving substitution in the 8-fold coordinated site. Most of the compositions vary in a range defined by the following recalculated formulae:

$$(Ca_{0.67}Mg_{0.07}REE_{0.06}Y_{0.01}Th_{0.13}U_{0.03})_{\Sigma 0.97}$$
$$(Zr_{1.06}Hf_{0.01})_{\Sigma 1.07} \ (Ti_{1.72}Fe_{0.23}Si_{0.01})_{\Sigma 1.96} \ O_{7.00}$$

$$(Ca_{0.62}Mg_{0.10}REE_{0.03}Y_{0.01}Th_{0.21}U_{0.04})_{\Sigma 1.09}$$
$$(Zr_{0.95}Hf_{0.01})_{\Sigma 0.96} \ (Ti_{1.75}Fe_{0.26}Si_{0.02})_{\Sigma 2.03} \ O_{6.92}.$$

Composition of the Zr–Th–U minerals

Baddeleyite (Table 2) is almost stoichiometric ZrO_2, with trace amounts of Ti (0.65 wt% TiO_2) and Fe (0.73 wt% FeO) substituting for Zr. Hf was detected only in a few cases, whereas the REE were invariably close to the detection limit. The grains of baddeleyite included in amphibole proved to have a distinctive composition characterized by anomalous enrichment in Th (39.17–42.76 wt% ThO_2) and U (8.38–5.60 wt% UO_2), and lower concentrations of Ca, Ti, Si, Fe, and Pb. The formula of the unusual baddeleyite can be recalculated to:

$$(Zr_{0.63}Th_{0.25}U_{0.05}Ti_{0.03}Si_{0.03}Pb_{0.01})_{\Sigma 1.00} \ O_{2.00}.$$

The oxides of the thorianite–uraninite series form two separate groups of compositions (Table 2). One consists of ThO_2–UO_2 intermediate compounds straddling the compositional limit between thorianite and uraninite. The other approaches more closely the composition of pure uraninite. Both minerals are characterized by minor substitution of other elements. Intermediate members of the thorianite–uraninite solid solution contains Pb, from 1.5 to 3.02 wt% PbO, and is

tected in a few samples. The compositions of the Finero zirconolite were recalculated assuming different schemes of substitution among the various elements (Bayliss *et al.* 1989). Although Mg is commonly as-

cribed to the Ti site, the most satisfactory approach to the ideal formula $CaZrTi_2O_7$ was achieved by adding Mg to the Ca site, together with Th, U, REE and Y, whereas Si and Fe were added to the Ti, and the trace
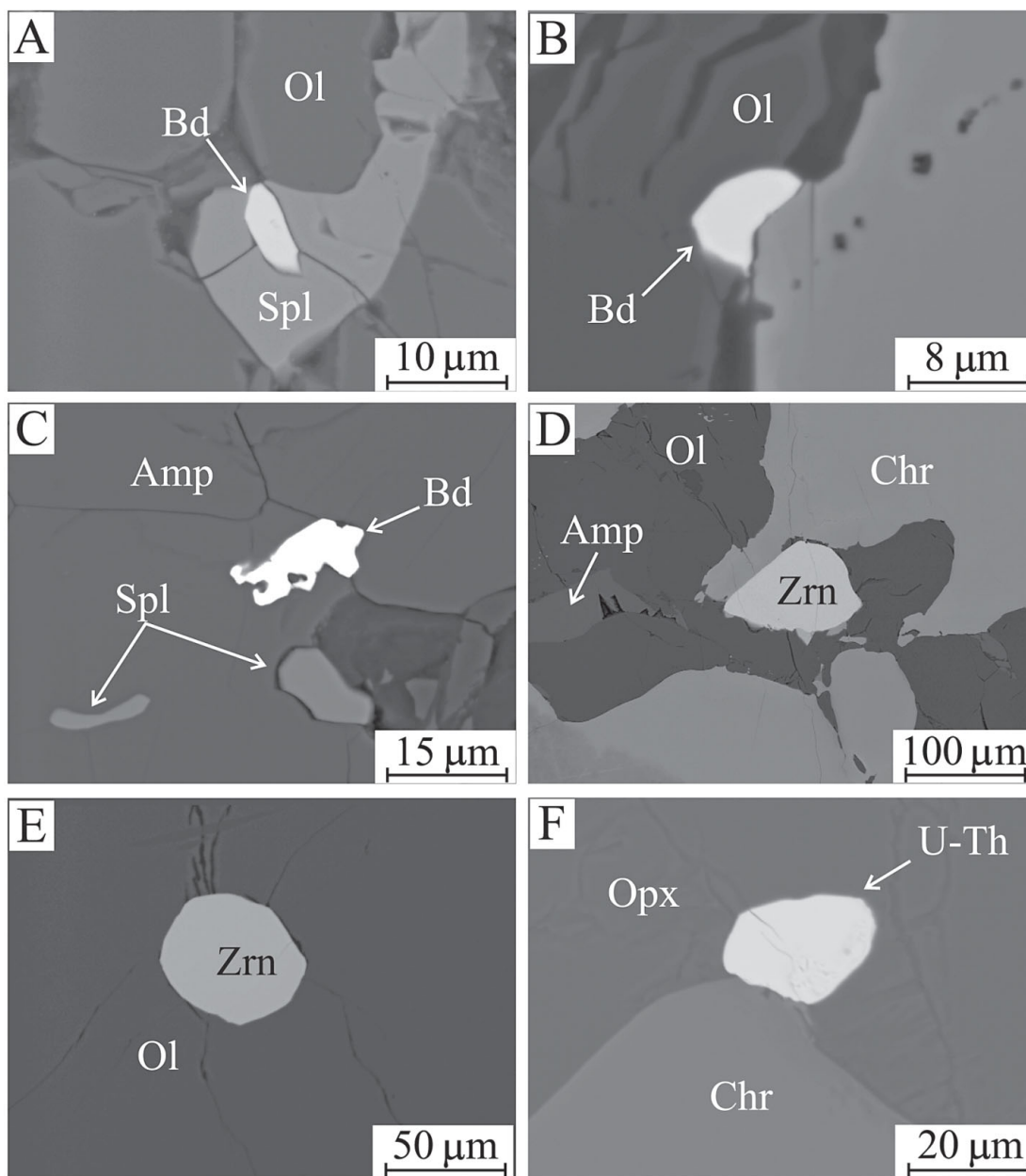
FIG. 6.   Textural relations of Zr–Th–U minerals in the Finero chromitites (BSE images). A) Baddeleyite surrounded by Fe–Al spinel interstitial to olivine. B) Baddeleyite in contact with massive chromite and olivine. C) Baddeleyite with high Th content associated with Fe–Al spinel, in amphibole. D) Uraninite–thorianite in contact with massive chromian spinel and orthopyroxene. E) Large grain of zircon in contact with massive chromian spinel and olivine. F) Zircon included in olivine. Symbols: Bd: baddeleyite, U–Th: uraninite–thorianite , Zrn: zircon, amp: amphibole; see Figure 2 for other symbols.

TABLE 1. SELECTED RESULTS OF ELECTRON-MICROPROBE ANALYSES OF ZIRCONOLITE
FROM CHROMITITE, FINERO COMPLEX, WESTERN ALPS, ITALY

|	MgO	SiO$_2$	CaO	TiO$_2$	FeO	Y$_2$O$_3$	ZrO$_2$	La$_2$O$_3$	Ce$_2$O$_3$	Pr$_2$O$_3$	Nd$_2$O$_3$	HfO$_2$	PbO	ThO$_2$	UO$_2$	Sum
D.L.	0.04	0.07	0.02	0.02	0.07	0.10	0.07	0.10	0.10	0.09	0.12	0.22	0.23	0.09	0.57	
CR1340C 11 1	n.d.	0.30	7.42	28.0	6.33	0.64	25.8	n.d.	n.d.	n.d.	n.d.	<0.2	0.23	9.51	12.1	90.33
PO1337B 1 1	0.99	0.11	9.80	35.9	4.86	0.54	32.2	0.22	0.48	<0.09	1.16	0.24	<0.2	11.6	3.17	101.27
PO1337B 1 2	0.99	0.21	9.35	35.9	5.03	0.70	32.4	<0.10	0.52	<0.09	0.96	0.57	<0.2	11.7	2.64	100.97
PO1337B 1 3	0.71	0.17	9.71	36.7	5.18	0.50	32.3	0.26	0.36	<0.09	0.73	<0.2	<0.2	9.96	2.46	99.04
PO1337B 1 8	n.d.	0.11	10.1	36.4	4.87	0.57	32.0	n.d.	n.d.	n.d.	n.d.	<0.2	0.58	11.0	3.45	99.08
PO1337B 2 1	0.95	0.16	9.57	37.0	5.18	0.51	31.0	0.14	0.28	<0.09	0.94	0.39	<0.2	12.2	2.95	101.27
PO1337B 2 2	0.98	0.27	8.88	35.5	4.80	0.29	29.6	0.12	0.54	<0.09	0.57	0.28	<0.2	13.8	2.60	98.23
PO1337B 2 3	n.d.	0.25	10.4	37.5	5.31	0.79	31.9	n.d.	n.d.	n.d.	n.d.	<0.2	<0.2	10.7	1.83	98.68
PO1337B 2 6	n.d.	0.23	9.58	36.8	5.14	0.34	30.8	n.d.	n.d.	n.d.	n.d.	<0.2	<0.2	12.3	3.25	98.44
PO1337C 1 1	0.80	0.27	9.20	33.4	4.28	0.66	30.5	0.22	0.64	<0.09	1.69	0.56	0.34	8.52	1.07	92.15
PO1337C 2A 1	0.79	0.22	10.2	35.0	4.47	0.50	32.2	<0.10	0.94	<0.09	1.19	0.30	0.26	9.10	1.40	96.57
PO1337C 4 1	0.92	0.33	9.41	33.9	4.91	0.62	32.7	<0.10	0.93	<0.09	1.41	0.22	<0.2	9.50	1.01	95.86
PO1360 1 1	0.67	0.32	8.84	33.4	6.75	0.56	31.9	0.35	0.75	<0.09	1.37	0.28	<0.2	11.2	3.65	100.04
PO1360 2A 1	0.70	0.09	9.82	36.0	4.41	0.40	34.4	0.31	0.93	<0.09	1.38	0.41	<0.2	8.77	1.77	99.39
PO1360 2B 1	0.75	0.07	10.3	37.6	4.48	0.70	33.2	0.22	0.77	<0.09	1.15	0.48	0.24	10.3	1.67	101.93
PO1360 4A 1	0.85	0.32	9.35	36.1	4.71	0.60	33.0	0.25	0.85	<0.09	1.52	0.47	<0.2	9.03	2.11	99.16
PO1360 4B 1	1.70	0.93	8.98	33.9	4.89	0.37	31.0	0.30	0.70	<0.09	1.18	<0.2	0.54	10.2	2.91	97.60
PO1364 10 1	1.77	1.43	8.81	29.8	5.20	0.63	27.3	0.18	0.76	0.15	1.30	0.70	<0.2	9.73	3.95	91.71

D.L.: detection limit, n.d.: not determined.

relatively enriched in REE, with Ce (2.02 wt% Ce$_2$O$_3$) prevailing over Nd (0.68 wt% Nd$_2$O$_3$) and La (0.36 wt% La$_2$O$_3$). The compositions vary between the recalculated formulae:

$$(Th_{0.43}U_{0.48}Pb_{0.03}Ce_{0.03}Nd_{0.01}Ca_{0.02}Fe_{0.01})_{\Sigma1.01} O_{1.99}$$

$$(Th_{0.48}U_{0.45}Pb_{0.03}Ce_{0.03}Nd_{0.01}Ca_{0.02})_{\Sigma1.02} O_{1.98}.$$

The uraninite is characterized by high Pb contents and a slight oxygen deficiency, approaching the formula: $U_{0.8}Pb_{0.25}Th_{0.02}O_{1.93}$.

The zircon is almost pure $ZrSiO_4$, with up to 1.13 wt% HfO$_2$ and trace amounts of Y (0.25 wt% Y$_2$O$_3$) substituting for Zr (Table 2). The thorium silicate, thorite or huttonite (Table 2), is quite homogeneous with small amounts of U (1.8 wt% UO$_2$), Pb (0.71wt% PbO), Fe (0.25 wt% FeO) and REE (0.77 wt% La$_2$O$_3$, 0.94 wt% Ce$_2$O$_3$). The approximate formula can be recalculated to:

$$(Th_{0.90}U_{0.02}Pb_{0.01}Ce_{0.02}La_{0.01}Fe_{0.01})_{\Sigma0.97} Si_{1.03} O_{4.00}.$$
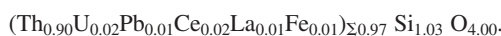
COMPARISON WITH ZIRCONOLITE OCCURRENCES WORLDWIDE

An overview of worldwide occurrences of zirconolite, modified after Williams & Gieré (1996) and Gieré
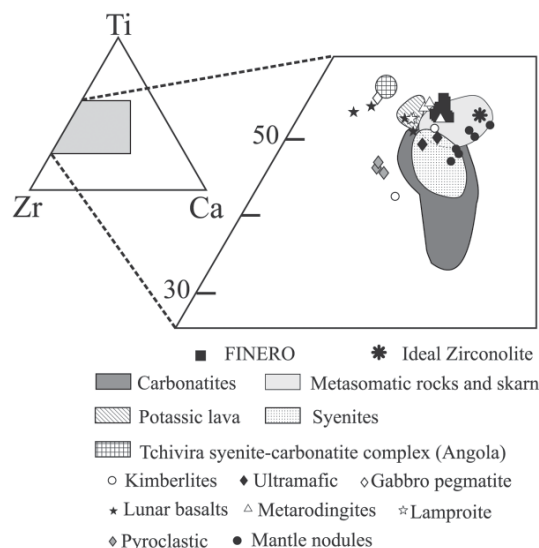

FIG. 7. Ca–Zr–Ti composition (at.%) of zirconolite from the Finero compared with compositions of zirconolite occurrences worldwide (Table 3). Data from: Busche *et al.* (1972), Williams & Gieré (1996), De Hoog & van Bergen (2000), Della Ventura *et al.* (2000), Stucki *et al.* (2001), Carlier & Lorand (2003). Individual symbols: occurrences with less than 10 compositions.

TABLE 2. SELECTED RESULTS OF ELECTRON-MICROPROBE ANALYSES OF BADDELEYITE AND Zr-Th-U MINERALS FROM CHROMITITE, FINERO COMPLEX, WESTERN ALPS, ITALY

	MgO	SiO$_2$	CaO	TiO$_2$	FeO	Y$_2$O$_3$	ZrO$_2$	La$_2$O$_3$	Ce$_2$O$_3$	Pr$_2$O$_3$	Nd$_2$O$_3$	HfO$_2$	PbO	ThO$_2$	UO$_2$	Sum
D.L.	0.04	0.07	0.02	0.02	0.07	0.10	0.07	0.10	0.10	0.09	0.12	0.22	0.23	0.09	0.57	
Baddeleyite																
PO1337B 4 1	0.11	<0.07	<0.02	<0.02	<0.07	<0.10	100.5	<0.10	<0.10	0.09	<0.12	<0.22	<0.23	<0.09	<0.57	100.70
PO1337B 4 1	n.d.	0.07	<0.02	0.51	0.63	<0.10	99.8	n.d.	n.d.	n.d.	n.d.	n.d.	<0.23	<0.09	<0.57	101.01
PO1337B 4 2	n.d.	0.18	<0.02	0.48	0.63	<0.10	99.1	n.d.	n.d.	n.d.	n.d.	n.d.	<0.23	<0.09	<0.57	100.39
PO1337B 5 1	n.d.	0.21	<0.02	0.51	0.75	<0.10	99.0	n.d.	n.d.	n.d.	n.d.	n.d.	<0.23	<0.09	<0.57	100.47
PO1337B 7 1	n.d.	0.17	0.03	0.66	0.67	<0.10	99.2	n.d.	n.d.	n.d.	n.d.	n.d.	<0.23	<0.09	<0.57	100.73
PO1364 1 1	0.05	0.10	0.02	0.45	0.73	<0.10	97.4	0.12	<0.10	<0.09	<0.12	0.34	<0.23	<0.09	<0.57	99.21
PO1364 2a 1	n.d.	0.33	0.02	0.37	0.54	<0.10	95.8	n.d.	n.d.	n.d.	n.d.	n.d.	0.23	<0.09	<0.57	97.29
PO1364 2b 1	n.d.	0.84	<0.02	0.48	0.92	<0.10	91.6	n.d.	n.d.	n.d.	n.d.	n.d.	<0.23	<0.09	<0.57	93.84
PO1364 4 1	0.16	0.50	<0.02	0.65	0.67	<0.10	93.4	0.13	<0.10	<0.09	<0.12	<0.22	<0.23	<0.09	<0.57	95.51
PO1364 11 1	0.09	0.37	0.07	0.42	0.54	<0.10	97.4	<0.10	<0.10	<0.09	0.39	<0.22	<0.23	0.16	<0.57	99.44
PO1364 12 1	0.09	0.26	0.03	0.46	0.58	<0.10	98.0	<0.10	0.15	0.12	0.19	<0.22	<0.23	<0.09	<0.57	99.88
PO1364 8 2	<0.04	0.97	0.44	1.24	0.14	0.10	45.7	0.10	<0.10	0.13	0.12	0.22	1.00	38.2	7.16	95.52
PO1364 9 1	<0.04	0.95	0.24	1.20	0.22	0.10	44.3	<0.10	<0.10	0.14	<0.12	<0.22	0.70	40.7	5.94	94.49
PO1364 9 2	n.d.	0.70	0.33	1.20	0.25	0.15	42.4	n.d.	n.d.	n.d.	n.d.	n.d.	0.82	40.1	5.81	91.76
PO1364 9 3	n.d.	0.96	0.25	1.29	0.19	<0.10	44.3	n.d.	n.d.	n.d.	n.d.	n.d.	0.96	41.7	7.23	96.88
PO1364 9 4	n.d.	1.05	0.24	1.20	0.27	0.13	43.7	n.d.	n.d.	n.d.	n.d.	n.d.	0.99	41.5	5.43	94.51
Zircon																
CR1340C 7B 1	<0.04	33.7	<0.02	<0.02	0.14	0.25	63.6	<0.10	<0.10	<0.09	0.12	1.13	<0.23	<0.09	<0.57	98.94
CR1340C 7C 1	<0.04	34.7	<0.02	<0.02	0.19	<0.10	62.5	<0.10	<0.10	<0.09	<0.12	0.92	<0.23	0.09	<0.57	98.40
CR1340C 7C 2	0.05	33.1	0.02	<0.02	0.18	0.12	63.8	<0.10	<0.10	<0.09	0.12	0.97	<0.23	<0.09	<0.57	98.36
CR1340C 7C 3	<0.04	33.7	<0.02	<0.02	0.10	0.13	65.9	<0.10	<0.10	<0.09	<0.12	0.99	<0.23	<0.09	<0.57	100.82
Thorianite–Uraninite																
CR1340A 1A 1	0.04	0.17	0.39	0.06	<0.07	<0.10	0.08	0.10	1.20	0.18	0.65	<0.22	2.41	48.3	46.2	99.78
CR1340A 1A 2	n.d	<0.07	0.40	0.03	0.10	<0.10	<0.07	n.d	n.d	n.d	n.d	<0.22	3.02	48.6	49.7	101.85
CR1340A 1A 3	0.04	0.23	0.52	0.07	0.18	<0.10	0.09	0.15	0.68	<0.09	0.43	<0.22	2.35	43.5	51.0	99.24
CR1340A 1A 4	n.d	0.11	0.48	0.04	0.19	<0.10	0.12	n.d	n.d	n.d	n.d	<0.22	2.21	46.1	48.2	97.45
CR1340A 1A 5	0.04	0.17	0.40	0.02	0.13	<0.10	0.07	<0.10	0.79	0.33	0.28	<0.22	2.58	47.1	47.3	99.21
CR1340A 1B 1	0.08	<0.07	0.39	0.08	0.21	<0.10	0.23	0.25	1.64	0.20	0.60	<0.22	2.46	44.1	48.5	98.74
CR1340A 1B 4	<0.04	0.13	0.33	<0.02	0.22	<0.10	0.08	0.36	2.02	0.16	0.68	<0.22	2.47	42.3	48.9	97.65
CR1340A 1B 6	n.d	0.11	0.34	0.05	0.37	0.18	<0.07	n.d	n.d	n.d	n.d	<0.22	2.03	48.0	50.5	101.58
CR1340 6 4	0.07	<0.07	0.36	0.07	0.33	0.10	0.07	0.16	0.92	0.20	0.23	<0.22	2.05	54.5	40.9	99.96
CR1340 3 5	0.06	<0.07	0.31	<0.02	0.21	0.11	0.18	0.13	0.44	<0.09	0.12	<0.22	1.50	64.7	32.9	100.66
CR1340 1 75	<0.04	<0.07	0.27	0.06	0.66	0.10	0.15	<0.10	0.67	<0.09	<0.12	<0.22	1.92	59.2	35.5	98.53
CR1340 1 38	0.04	0.32	0.64	0.05	0.13	<0.10	<0.07	<0.10	0.78	<0.09	0.14	<0.22	18.0	1.14	77.0	98.24
CR1340 1 39	0.04	0.13	0.13	0.04	0.11	<0.10	<0.07	0.11	0.91	<0.09	0.12	<0.22	19.2	1.84	75.9	98.53
Thorite or Huttonite																
PO1364 5 1	<0.04	19.7	0.04	<0.02	0.25	0.19	<0.07	0.77	0.94	0.17	0.12	<0.22	0.71	75.3	1.80	99.99
PO1364 5 2	<0.04	20.3	0.04	<0.02	0.23	<0.10	<0.07	0.82	1.03	0.11	0.12	<0.22	0.47	74.5	0.71	98.33
PO1364 5 8	<0.04	19.5	<0.02	<0.02	0.32	<0.10	<0.07	0.58	0.70	0.11	0.12	<0.22	1.07	76.9	0.57	99.87
PO1364 5 9	<0.04	20.0	0.03	<0.02	0.38	0.14	<0.07	0.83	1.01	0.11	0.15	<0.22	1.17	73.8	1.09	98.71
CR1340 13 7	<0.04	14.6	0.16	<0.02	0.43	0.12	<0.07	0.22	0.34	<0.09	<0.12	<0.22	0.56	82.6	1.60	100.63
CR1340 4 8	<0.04	15.6	0.08	<0.02	0.22	0.10	<0.07	0.13	0.22	<0.09	<0.12	<0.22	0.23	82.5	1.18	100.26
CR1340 1 4	<0.04	15.6	0.08	<0.02	0.61	<0.10	<0.07	<0.10	0.14	<0.09	<0.12	<0.22	0.43	82.7	1.56	101.12
CR1340 1 6	<0.04	15.6	0.04	<0.02	0.33	<0.10	<0.07	0.11	0.14	<0.09	<0.12	<0.22	0.20	81.8	1.67	99.89
CR1340 1 7	<0.04	15.7	0.04	<0.02	0.42	<0.10	<0.07	0.11	0.16	<0.09	<0.12	<0.22	0.23	82.6	0.99	100.25

D.L.: detection limit, n.d.: not determined.

et al. (1998), is given in Table 3. The compositions are plotted in terms of Ca–Ti–Zr, together with those obtained from the Finero chromitites (Fig. 7). The diagram shows that natural samples deviate significantly from the theoretical stoichiometry, and diverge with an increasing proportion either in the Ca or the Ti site, or both, whereas the extent of Zr substitution is generally very limited (Harley 1994). This permits accommodation of various elements in the structure, so that the composition of natural zirconolite can be described in terms

of the following five end-members: $CaZrTi_2O_7$, (ACT)$ZrTiMe^{2+}O_7$, (REE)$ZrTiMe^{3+}O_7$, (REE)$ZrMe^{5+}Me^{2+}O_7$, and $CaZrMe^{5+}Me^{3+}O_7$, where: ACT = Th + U, Me^{2+} = Mg + Mn + Fe^{2+}, Me^{3+} = Fe^{3+} + Al + Cr, and Me^{5+} = Nb + Ta (Gieré *et al.* 1998). These authors have shown that type and extent of substitution are strongly dependent on the geochemical environment of formation, and distinct compositional groups can be defined for specific rock-associations or individual geological localities (Table 3). Most of the substitution in the

TABLE 3. OCCURRENCES, PREDOMINANT SUBSTITUTIONS
AND PARAGENESES OF ZIRCONOLITE*

Rock type	*n*	Locality	Predominant substitution	Paragenetic assemblage
Chromitite	2	Finero (Italy)	(Th, U, REE, Me^{2+})	Ap, Bd, Chr, Cpx, Ilm, Mgt, Mlb, Ncu, Ol, Opx, Phl, Pn, Rt, Thn, Thr-Hut, Urn, Zrn
		Cuba	(Y, REE, Me^{2+})	Ap, Chr, Hbl, Ilm, Mgt, Ol, Opx, Pl, Rt, Sulf
Alnoite	1	Québec (CAN)	No data	Bd, Prv
Anorthosite	1	Skaergaard (Greenland)	No data	Aln, Ap, Bd, Ilm, Pl, Ttn, Zrn
Calc-alkaline lava	1	Indonesia	(Y, REE, Me^{3+}, Th, U, Nb)	Kfs, Si
Carbonatite	16	Kovdor (Russia)	(Nb, Ta)	Ap, Bd, Clz, Chu, Mgt
		Howard Creek (CAN)	(Th, U, REE, Me^{2+})	Prv, Pch, Rt, Whl, Zrn
		Phalaborwa (RSA)	(Th, U, Me^{2+})	
		Araxà (Brazil)	(Nb, Ta, REE)	
Cordierite gneiss	1	Ontario (CAN)	No data	Rt, Ttn, Zrn
Gabbro pegmatite	1	Scotland	(Y, REE, Me^{2+})	Aln, Ap, Bt, Ep, Ttn, Zrn
Kimberlite	3	South Africa	(only major elements)	Bd, Cal, Ilm, Zrn
Lamproite	1	Peru	(REE, Th, Me^{2+})	Ap, Chr, Cpx, Kfs, Ilm, Ol, Opx, Phl, Po, Py
Metasomatic Carbonate Rocks	11	Adamello (Italy)	(Th, U, REE, Me^{2+}, Me^{3+})	Aln, Ap, Bd, Bet, Cal, Chl
		Oetztal–Stubai (Austria)	(Nb, Y, Me^{2+}, Me^{3+})	Chu, Cpx, Dsk, Dol, Gek, Ilm, Jrd, Ol, Opx, Phl, Po, Py, Rsb, Rt, Spl, Ttn, Zrn
Metasomatic	1	Antartica	(Nb, REE, Me^{2+})	Ap, Ilm, Lct, Ne, Phl, Pl,
Mantle Xenolith	1	South Africa	(only major elements)	Bd, Ol, Opx, Spl, Zrn, MARID
Metarodingite	1	Alps (Italy)	(REE, Y, Me^{2+})	Ap, Bd, Chl, Cpx, Hbl, Ilm, Ol, Spl, Zrn
Sapphirine Granulite	1	Antarctica	(Y, REE, Me^{2+}, Me^{3+})	Opx, Phl, Spr, Spl
Syenite and Nepheline Syenite	12	Norway	(Nb, REE, Th, U)	Aln, Ap, Bd, Bt, Ep, Hln
		Angola	(Y, REE, Me^{2+}, Me^{3+})	Hbo, Ilm, Mgt, Mnz, Prv, Pbk, Ttn, Whl, Zrn
Placer	2	Jacupiranga (Brazil) Sri Lanka	Various	Bd, Prv
Ultrabasic Rocks	3	Laouni (Algeria)	(Me^{2+}, Y, REE)	Ap, Bd, Zrn
		Rhum (Scotland, U.K.)	No data	
Lunar Basalts	7	Various landing sites	(REE, Hf, Me^{2+}, Me^{3+})	Bd, Ilm, Ol, Pl
Meteorite	1	Allende carbonaceous chondrite	incomplete analysis	Prv, Ol, Pl

* Sources of data: Williams & Gieré (1996); Gieré *et al.* (1998); see text for further references.

n: number of reported occurrences; Me^{2+}: Fe^{2+}, Mg, Mn; Me^{3+} = Fe^{3+}, Cr, Al.

Mineral symbols: Aln: Allanite, Ap: Apatite, Bd: Baddeleyite, Bet: Betafite, Bt: Biotite, Cal: Calcite, Clz: Calzirtite, Chl: Chlorite, Chu: Clinohumite, Cpx: Clinopyroxene, Chr: Chromian spinel, Dsk: Dissakisite, Dol: Dolomite, Ep: Epidote, Gek: Geikielite, Hln: Hellandite, Hbo: Hibonite, Hbl: Hornblende, Hut: Huttonite, Ilm: Ilmenite, Jrd: Jordisite, Kfs: K-feldspar, Lct: Leucite, Mgt: Magnetite, Mlb: Molybdenite, Mnz: Monazite, Ncu: Native copper, Ne: Nepheline, Ol: Olivine, Opx: Orthopyroxene, Pbk: Pseudobrookite, Prv: Perovskite, Phl: Phlogopite, Pl: Plagioclase, Pn: Pentlandite, Po: Pyrrhotite, Py: Pyrite, Pch: Pyrochlore, Rsb: Rosenbushite, Rt: Rutile, Spr: Sapphirine, Si: Amorphous silica, Spl: Spinel, Sulf: Sulfides, Thn: Thorianite, Thr: Thorite, Ttn: Titanite, Urn: Uraninite, Whl: Wöhlerite, Zrn: Zircon, MARID: Mica – Amphibole – Rutile – Ilmenite – Diopside metasomatic assemblage.

Finero samples occurs at the Ca site, whereas the less important substitution at the Ti site involves Si and Fe^{2+}, in the absence of Nb and Ta. Compositions have thus been plotted in the Ca – (REE + Y) – (U + Th) central section of the double tetrahedron (Fig. 8). The low REE + Y and relatively high (U + Th) content of the Finero material reveal similarities with zirconolite from carbonatites and metasomatic carbonate rocks. However, it differs markedly from zirconolite reported from mantle xenoliths (Horning & Wörner 1991), mafic–ultramafic layered intrusions of Scotland and Algeria (Williams 1978, Fowler & Williams 1986, Lorand & Cottin 1987), metarodingites (Stucki *et al.* 2001) and from the Lewotolo K-rich lavas (Indonesia) extruded in a subduction zone (De Hoog & van Bergen 2000) (Fig. 8). Comparison with zirconolite from the Cuba chromitites was not possible because of the lack of analytical data. However, substitution in the Ca site of the Cuba zirconolite is reported to be dominated by Y and REE, with very low contents of Th and U (Proenza *et al.* 2001); thus it differs significantly from the Finero compositions.

Variations in the Ca–Th–U diagram (Fig. 9) better define the affinity of the Finero zirconolite with compositions from carbonatite association, and its differences from zirconolite in metasomatic carbonate rocks from contact skarns (Gieré 1990, Gieré & Williams 1992). In fact, there are distinct similarities with zirconolite from some carbonatite complexes in which Th + U substitution for Ca is predominant (Fig. 10A), and in particular with those from Howard Creek, British Columbia, Canada, which display simultaneous enrichment in U and Th, similar to that at Finero (Fig. 10B).

CONSTRAINTS ON THE FORMATION OF THE FINERO ZIRCONOLITE

The occurrence of zirconolite in the upper mantle was first documented from metasomatized xenoliths in kimberlite or basanite. There it occurs as either an "exotic" reaction-induced phase (Haggerty 1987, 1995) or as a constituent of an ultrapotassic assemblage in veins cutting across a dunite fragment (Horning & Wörner 1991). The Finero zirconolite and the Zr–Th–U minerals (baddeleyite, zircon, thorianite, uraninite, thorite or huttonite) occur in chromitites associated with a large orogenic upper-mantle massif, unrelated to late veins or fractures. The minerals are part of the accessory metasomatic assemblage phlogopite + amphibole + (Mg,Ca) carbonates + apatite + ilmenite + rutile + (Fe,Al)-rich spinel that formed during the pervasive metasomatism of the Finero mantle. Textural relations indicate that the metasomatic minerals formed by a sequence of crystallization events during the metasomatic process. Phlogopite and (Mg,Ca) carbonates are almost exclusively included in chromian spinel. Other phases, such as am-
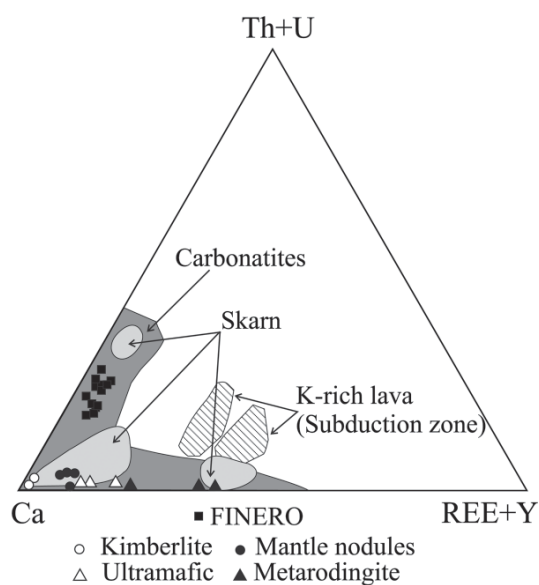

FIG. 8. Ca – (Th + U) – (REE + Y) composition (at.%) of zirconolite from the Finero complex compared with compositional fields of zirconolite from carbonatites, metasomatic skarns (Williams & Gieré 1996), mafic–ultramafic rocks (Williams 1978, Lorand & Cottin 1987), mantle nodules (Horning & Wörning 1991), metarodingites (Stucki *et al.* 2001), and the Lewotolo K-rich lavas (Indonesia) emplaced in a suprasubduction zone (De Hoog & van Bergen 2000).
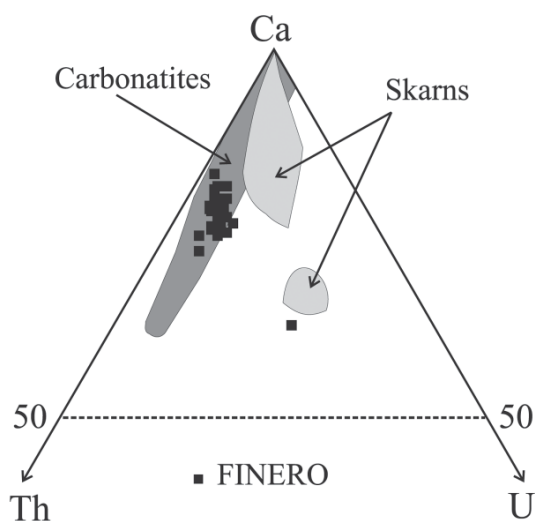

FIG. 9. Ca–U–Th composition (at.%) of zirconolite from the Finero complex compared with zirconolite from carbonatites and metasomatic carbonate rocks (skarns). Source of data: Williams & Gieré (1996).
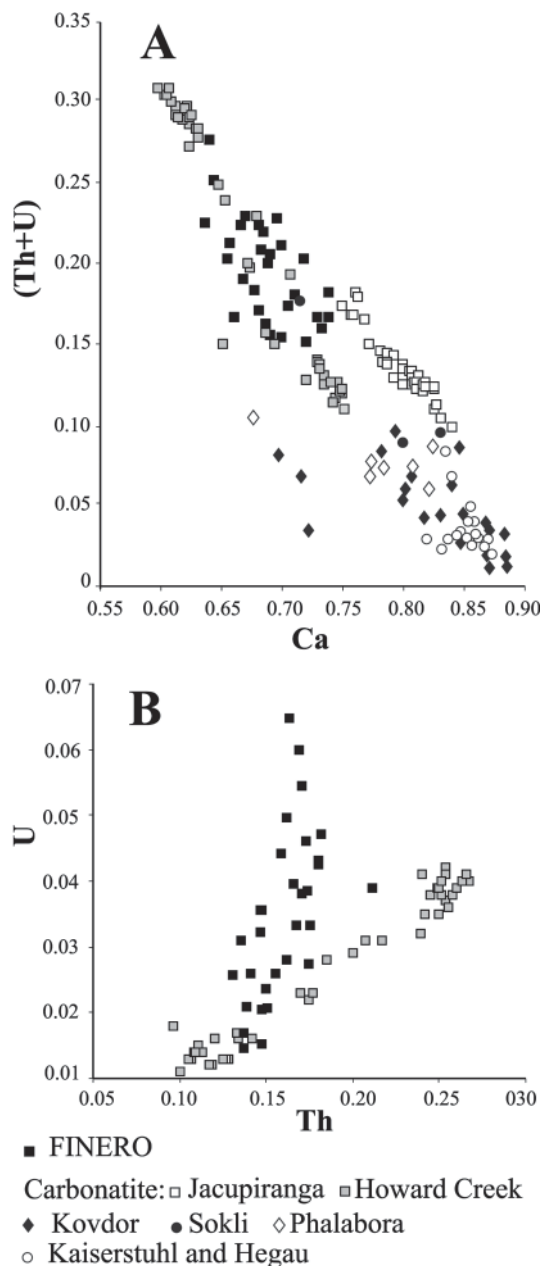
FIG. 10.   A) Ca – (Th + U) covariation in zirconolite from Finero and selected carbonatite complexes, characterized by predominant (Th + U)-for-Ca substitution. B) Th–U positive correlation in zirconolite from the Finero chromitite and the Howard Creek carbonatite. Source of data: Williams & Gieré (1996); the data of Jacupiranga were deduced from Figure 4 in Bellatreccia *et al.* (1999).

phibole, rutile and ilmenite, occur either included in chromian spinel or associated with the silicate ground-mass. Zircon, thorianite, and uraninite crystallized interstitially to chromian spinel or at the contact between chromian spinel and mafic silicates, but are not necessarily related to the symplectite reaction-zones at the chromian spinel – silicate boundary nor with (Al,Fe)-rich spinel. In contrast, zirconolite is invariably associated with symplectite and blebs of (Al,Fe)-rich spinel, along with apatite, ilmenite, and rutile. Baddeleyite occurs in the same textural position as zircon, but also with zirconolite in composite grains, or even as monophase inclusions in amphibole of the silicate matrix, far from the massive chromian spinel, and in this case, it is remarkably enriched in Th.

Thus the assemblage of metasomatic minerals, and in particular the Zr–Th–U minerals, are found in paragenetic association with compositionally distinct spinel–olivine pairs (Tables 4, 5). The order of crystallization suggests that they reached equilibration of the Mg–Fe^{2+} exchange, under different conditions of oxygen fugacity and temperature. The results of spinel–olivine thermobarometry (Ballhaus *et al.* 1991), at an assumed pressure of 1.0 GPa compatible with the spinel-peridotite facies of the Finero mantle, are illustrated in Figure 11. The relationships between temperature and oxygen fugacity indicate that massive chromitite equilibrated in a wide thermal interval between 1150 and 700°C and in a relatively narrow range of oxygen fugacities, from +1.7 to –1.0 Δlog $f(O_2)$ units, *i.e.*, in the vicinity of the FMQ buffer. Metasomatic minerals such as phlogopite, amphibole and (Mg,Ca) carbonates occur as inclusions in the high-T chromian spinel. The metasomatic reaction with alkaline fluids thus most likely started at temperatures on the order of 1100°C. The olivine – chromian spinel pairs in contact with zircon give temperatures at the low-T end of this trend. The olivine – (Fe,Al)-spinel symplectites with zirconolite, baddeleyite and apatite gave temperatures of formation from 800°C to less than 600°C, at oxygen fugacities decreasing from 1.8 log units above the FMQ, down to –3.2 log units below it. A minimum of –7.5 Δlog $f(O_2)$ is recorded by olivine–spinel symplectite pairs associated with apatite but no Zr–Ti phases.

The composition of the metasomatic minerals and the inferred variation of oxygen fugacity with decreasing temperature apparently reflect fractionation of the volatile component and associated incompatible elements. The fractionation trend involves initial segregation of F, H$_2$O and CO$_2$, together with K, Na, and Ba, at about 800°C. With decreasing temperature, the volatile component became enriched in Cl, P and CO$_2$, whereas the activity of the LREE, Zr, Pb, Th and U increased progressively in the fluid. This increase led to the precipitation of specific phases interstitial to chromite (zircon, thorianite, uraninite, baddeleyite), or in association with spinel symplectites (zirconolite, baddeleyite, apatite). Textural relations indicate that the symplectites are

TABLE 4. SELECTED RESULTS OF ELECTRON-MICROPROBE ANALYSES OF SPINEL-GROUP MINERALS FROM CHROMITITE, FINERO COMPLEX, WESTERN ALPS, ITALY

	SiO_2	TiO_2	Al_2O_3	FeO	Fe_2O_3	MgO	MnO	Cr_2O_3	NiO	ZnO	V_2O_3	Sum
D.L.	0.05	0.02	0.03	0.06	0.06	0.02	0.03	0.05	0.03	0.02	0.02	
Massive chromian spinel												
CR84 3	<0.05	0.63	14.4	16.6	4.56	11.6	0.05	51.1	0.16	<0.02	<0.02	99.10
CR1340A	0.12	0.68	15.6	15.9	3.94	12.1	0.26	50.4	0.17	0.20	0.10	99.47
CR1340C	<0.05	0.64	15.5	17.4	3.20	11.5	0.22	52.2	0.15	<0.02	0.07	100.88
FN7 4	0.03	0.49	18.7	14.8	3.45	13.4	0.27	49.1	0.04	n.d.	n.d.	100.28
PO86 1	<0.05	0.61	14.3	16.2	5.76	12.1	0.20	51.3	0.11	<0.02	<0.02	100.58
PO1337B 1	<0.05	0.57	17.2	16.7	2.95	12.3	0.17	51.5	0.08	0.02	0.11	101.60
PO1362 7	0.05	0.53	18.2	16.0	3.17	12.9	0.25	50.8	0.17	n.d.	n.d.	102.07
PO1364 4	0.15	0.47	17.0	15.2	3.31	12.9	0.28	50.5	0.13	n.d.	n.d.	99.94
RF85 1	<0.05	0.58	13.5	15.4	7.10	12.3	0.20	50.4	0.11	<0.02	<0.02	99.59
RF1398 2	0.10	0.39	16.4	15.7	4.71	12.6	0.27	50.2	0.19	n.d.	n.d.	100.56
RM84 11	<0.05	0.47	15.9	16.2	3.18	11.9	0.32	51.8	0.19	<0.02	<0.02	99.96
RM84 4	<0.05	0.39	15.9	15.4	3.68	12.2	0.36	50.8	0.10	<0.02	<0.02	98.83
RM84 5	0.06	0.32	12.5	17.5	5.02	10.8	0.23	53.6	0.08	<0.02	<0.02	100.11
Symplectite spinel												
CR1340C 7	0.05	0.38	15.6	17.5	2.50	10.9	0.21	51.5	0.15	0.07	0.11	98.97
CR1340C 11	0.12	0.37	17.2	21.6	5.96	8.13	0.34	44.1	0.15	0.13	0.10	98.20
PO1337B 5 1	0.25	0.37	12.4	23.6	12.3	6.33	0.39	42.3	0.25	0.12	0.16	98.45
PO1362 1A	0.84	0.32	21.9	14.9	4.25	15.0	0.31	43.0	<0.03	0.13	0.11	100.76
PO1362 7	1.59	0.29	18.3	14.7	3.83	14.6	0.30	46.8	0.05	0.38	0.12	100.96
PO1364 1	1.28	0.20	26.1	14.3	3.99	15.4	0.21	39.3	0.03	0.28	0.12	101.21
PO1364 4	0.89	0.24	16.2	17.1	3.21	11.8	0.22	48.3	<0.03	0.14	<0.02	98.10
PO1364 9	1.12	0.13	26.0	17.7	0.10	12.1	0.28	38.4	<0.03	0.56	<0.02	96.41
PO1364 12	0.05	0.51	19.2	14.7	3.26	13.6	0.34	49.3	<0.03	0.21	0.23	101.40
RF1398 2	0.25	0.29	19.8	15.3	4.63	13.1	0.32	46.1	<0.03	0.18	0.12	100.09

D.L.: detection limit, n.d.: not determined.

TABLE 5. SELECTED RESULTS OF ELECTRON-MICROPROBE ANALYSES OF OLIVINE FROM CHROMITITE, FINERO COMPLEX, WESTERN ALPS, ITALY

|	SiO_2	TiO_2	Al_2O_3	FeO	MnO	MgO	CaO	Cr_2O_3	NiO	ZnO	V_2O_3	Sum
D.L.	0.05	0.02	0.03	0.06	0.06	0.02	0.03	0.05	0.03	0.02	0.02	
CR1340A	40.8	0.03	<0.03	6.07	0.08	52.4	0.03	<0.05	0.58	<0.02	<0.02	99.99
CR84 11	39.8	<0.02	0.11	8.33	0.09	49.5	0.13	<0.05	0.37	<0.02	<0.02	98.33
CR84 4	40.9	<0.02	<0.03	6.00	0.06	52.6	<0.03	<0.05	0.43	<0.02	<0.02	99.99
CR84 5	41.0	<0.02	<0.03	7.58	0.10	51.9	<0.03	<0.05	0.37	<0.02	<0.02	100.95
FN11A 6	40.7	<0.02	<0.03	6.19	0.06	50.1	0.06	0.14	0.33	<0.02	<0.02	97.58
PO1337 B 6	42.7	0.04	<0.03	4.73	0.06	51.4	0.03	0.23	0.57	<0.02	<0.02	99.76
PO1360 1 3	41.2	0.06	<0.03	8.47	0.17	50.6	0.03	<0.05	0.21	0.06	<0.02	100.80
PO1360 4	41.2	0.03	<0.03	4.57	0.08	53.5	0.05	0.18	0.36	<0.02	0.05	100.02
PO1362 1a	44.4	<0.02	<0.03	5.29	0.10	49.6	<0.03	0.24	0.22	0.03	0.03	99.91
PO1362 7	44.9	0.07	<0.03	4.69	0.08	48.2	<0.03	0.42	0.31	<0.02	0.05	98.72
PO1364 10	41.8	0.03	<0.03	8.21	0.09	50.3	<0.03	<0.05	0.51	0.07	<0.02	101.01
PO1364 2	41.6	<0.02	0.13	4.22	<0.06	51.9	<0.03	0.34	0.33	<0.02	<0.02	98.52
PO1364 4	43.2	0.03	0.11	4.47	0.13	50.4	<0.03	0.13	0.54	<0.02	0.10	99.11
RF1398 2 1	41.4	0.03	<0.03	3.90	0.05	53.0	<0.03	0.54	0.51	<0.02	<0.02	99.43
RM84 11	40.1	<0.02	<0.03	6.20	0.10	52.2	<0.03	<0.05	0.57	<0.02	<0.02	99.17
RM84 4	40.3	<0.02	<0.03	7.14	0.11	51.2	0.03	<0.05	0.46	<0.02	<0.02	99.24
RM84 7	41.5	<0.02	<0.03	5.04	0.06	53.1	0.03	<0.05	0.54	<0.02	<0.02	100.27
RM85 21	41.7	<0.02	<0.03	5.35	0.08	52.9	<0.03	<0.05	0.60	<0.02	<0.02	100.63

D.L.: detection limit.
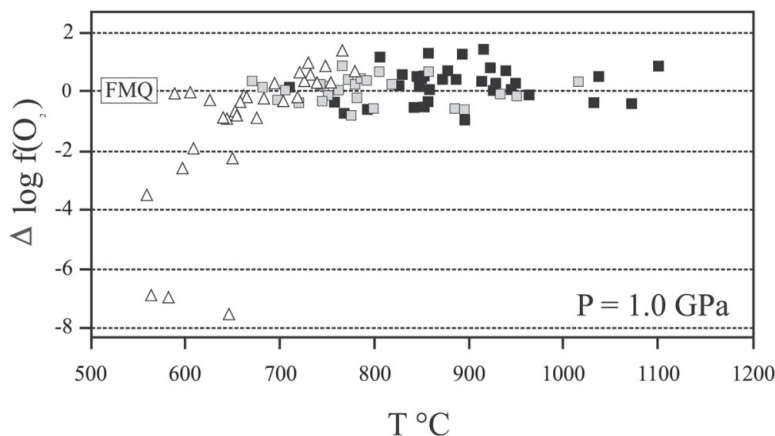
FIG. 11.   Variation of oxygen fugacity as function of temperature at 1.0 GPa, for olivine–
spinel pairs in the chromitites of Finero using the thermometer of Ballhaus *et al.* (1991).
Black squares: massive chromian spinel and interstitial olivine in zirconolite-free sam-
ples. Grey squares: massive chromian spinel and interstitial olivine in zirconolite-bear-
ing samples. Open triangles: spinel symplectite and olivine coexisting with baddeleyite,
zirconolite, and apatite.

TABLE 6. SELECTED RESULTS OF ELECTRON-MICROPROBE ANALYSES OF PHLOGOPITE INCLUSIONS
IN MASSIVE CHROMIAN SPINEL, FINERO COMPLEX, WESTERN ALPS, ITALY

	SiO_2	TiO_2	Al_2O_3	FeO	MnO	MgO	CaO	Na_2O	K_2O	SrO	BaO	Cr_2O_3	NiO	Cl	F	Sum
D.L.	0.04	0.02	0.03	0.06	0.03	0.02	0.10	0.01	0.01	0.04	0.04	0.06	0.03	0.02	0.03	
CR1340B 2	39.6	3.72	14.3	1.53	<0.0	25.7	0.10	0.98	9.43	<0.04	0.55	1.63	0.22	0.18	1.09	99.03
CR1340B 3	36.9	4.51	15.2	1.48	<0.0	23.3	<0.10	2.00	5.75	<0.04	6.71	1.97	0.12	0.15	0.78	98.87
CR86 9 1	39.1	2.48	14.9	1.74	<0.0	25.4	0.10	0.50	8.80	<0.04	0.11	1.93	0.21	0.10	1.04	96.41
CR86 9 2	40.6	2.73	14.8	1.82	0.03	25.3	<0.10	0.37	9.66	<0.04	0.08	1.60	0.16	0.23	0.61	97.99
CR86 9 3	39.0	1.80	14.8	1.62	<0.0	26.9	<0.10	0.11	9.43	<0.04	0.09	2.06	0.19	0.23	0.61	96.84
CR86 9 4	39.4	2.16	17.2	1.92	<0.0	24.1	0.12	1.29	7.83	<0.04	2.51	2.29	0.11	0.09	1.41	100.43
CR86 9 5	41.2	2.99	15.0	1.87	0.06	25.4	0.10	0.44	9.19	<0.04	1.32	1.51	0.13	0.21	0.93	100.35
FN11D 1	41.6	2.39	16.6	1.72	0.13	21.3	0.10	0.84	7.21	<0.04	2.08	1.83	0.14	0.12	1.92	97.98
PO1337C 3	38.3	0.52	16.1	1.19	<0.0	23.8	0.20	2.46	1.52	0.06	9.02	1.10	0.12	0.08	0.11	94.58
PO86 4	39.6	1.77	14.9	1.74	<0.0	25.7	0.10	0.25	10.1	<0.04	0.04	1.54	0.13	0.24	0.68	96.79
RM84 2	39.5	1.91	15.8	2.04	0.03	26.4	0.13	0.17	9.45	<0.04	0.04	1.38	0.15	0.02	0.36	97.38
RM84 5	40.2	0.55	13.0	2.18	<0.0	28.6	<0.10	0.30	8.70	<0.04	0.12	1.35	0.12	0.29	0.17	95.58
RM84 7	39.0	1.54	15.6	1.62	<0.0	27.2	<0.10	0.26	9.39	<0.04	0.05	1.55	0.03	0.21	0.23	96.68
(*)	39.9	0.97	16.0	2.73	0.03	24.5	<0.10	0.58	8.70	n.d.	0.31	1.16	0.16	0.03	0.10	95.17

D.L.: detection limit, n.d.: not determined. (*) Average composition of phlogopite from the Finero mantle peridotite (Exley *et al.* 1982).

the result of a late reaction due to instability of the pair chromian spinel – Mg silicate, induced by the increase of fluid activity in the system. Examination of the mineral assemblage in the symplectite suggests the formation of zirconolite according to the reaction suggested by Gieré *et al.* (1998):

baddeleyite + 2 rutile + calcite → zirconolite + CO_2.
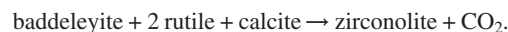
This reaction requires the initial presence in the metasomatic system of a carbonate component, and involves liberation of CO_2. The process implies that CO_2/H_2O ratios probably increased in the final stages of metaso-

TABLE 7. SELECTED RESULTS OF ELECTRON-MICROPROBE ANALYSES OF APATITE FROM CHROMITITE, FINERO COMPLEX, WESTERN ALPS, ITALY

	SiO₂	TiO₂	Al₂O₃	FeO	MnO	MgO	CaO	Na₂O	K₂O	Cr₂O₃	P₂O₅	SrO	BaO	La₂O₃	Ce₂O₃	Pr₂O₃	Nd₂O₃	Cl	F	Sum
D.L.	0.04	0.02	0.03	0.06	0.03	0.02	0.10	0.01	0.01	0.06	0.02	0.05	0.04	0.07	0.07	0.08	0.08	0.02	0.03	
PO1337B 1	0.31	<0.02	0.09	0.56	<0.03	0.26	55.2	0.09	<0.01	0.43	42.0	0.05	0.06	0.12	0.18	0.13	0.10	1.11	<0.03	100.69
PO1337B 2	0.93	<0.02	0.11	0.49	0.05	0.35	52.7	0.10	0.01	0.30	42.3	0.05	0.28	0.13	0.19	0.12	0.09	0.99	<0.03	99.19
PO1337B 3	0.38	<0.02	0.03	0.43	0.04	0.37	56.9	0.20	<0.01	0.21	42.1	<0.05	0.04	0.17	0.32	0.11	0.15	0.94	<0.03	102.39
PO1337B 4	0.43	0.02	0.04	0.41	0.04	0.44	56.6	0.04	0.01	0.17	42.3	0.06	<0.04	0.16	0.33	0.10	0.13	0.95	<0.03	102.23
PO1364 10 1	0.39	<0.02	0.16	0.40	0.10	0.27	51.3	0.03	<0.01	0.22	44.4	<0.05	<0.04	0.20	0.31	<0.08	0.11	0.77	<0.03	98.66
PO1364 10 2	0.45	<0.02	0.16	0.53	0.05	0.26	51.2	0.04	0.01	0.32	43.5	<0.05	<0.04	0.23	0.31	<0.08	0.14	0.65	0.73	98.58
PO1364 10 3	0.53	<0.02	0.15	0.55	0.14	0.50	51.4	0.03	<0.01	0.20	42.8	<0.05	<0.04	0.21	0.29	<0.08	0.13	0.71	<0.03	97.64
PO1364 10 4	0.35	<0.02	0.29	0.56	0.03	0.24	52.0	0.05	<0.01	0.41	43.0	<0.05	<0.04	0.19	0.27	<0.08	0.12	0.81	0.49	98.81
PO1364 10 5	0.67	<0.02	0.08	0.52	0.06	0.36	53.4	<0.01	<0.01	0.16	40.6	0.08	0.07	0.18	0.28	<0.08	0.15	0.54	0.09	97.24
RF1398 2 1	0.13	0.02	0.08	0.34	<0.03	0.25	54.3	<0.01	<0.01	0.64	43.0	0.06	<0.04	0.11	0.22	0.12	<0.08	0.38	<0.03	99.65
RF1398 2 2	1.76	0.04	0.25	0.39	0.05	0.96	56.6	<0.01	<0.01	0.66	37.5	<0.05	<0.04	0.14	0.24	0.11	<0.08	0.13	<0.03	98.83
RF1398 2 3	0.77	0.09	0.25	0.55	<0.03	0.54	53.8	<0.01	<0.01	0.78	41.5	<0.05	<0.04	0.10	0.25	0.10	<0.08	0.41	<0.03	99.14

D.L.: detection limit.

matism, contemporaneously with the observed change of the chemical-physical conditions from slightly oxidized to more reduced with progressive decrease in temperature.

THE METASOMATIC FLUID PHASE

Electron-microprobe compositions of accessory phlogopite and apatite in the Finero chromitites (Tables 6, 7) indicate that the fluid phase was enriched in H_2O, F, Cl, P_2O_5, with a significant proportion of CO_2, and was able to carry incompatible elements such as K, Na, Ba, Ti, Zn, Pb, Zr, REE, U, and Th.

Crystallization of the massive chromian spinel was accompanied by entrapment of phlogopite together with carbonate phases, at temperatures as high as 1100°C. Crystallization of carbonates continued in association with amphibole in the silicate matrix of the chromitite. CO_2 activity was high during crystallization of the spinel symplolite – zirconolite – baddelyite – apatite assemblage in the latest stages of metasomatism. The entire metasomatic cycle in the Finero chromitites occurred under relatively high activity of CO_2, suggesting that the metasomatic fluid was rich in an alkaline-carbonatite component. Additional evidence derives from the peculiar composition of phlogopite and apatite. Phlogopite inclusions in massive chromian spinel (Table 6) differ from the coarse-grained phlogopite in the mantle peridotite of Finero (Exley *et al*. 1982) in their higher Ti, Na, and Cr contents, and in their halogen (F + Cl) contents, from 0.1 to 2.04 wt%. Fluorine (0.1–1.9 wt%) is invariably higher than Cl (0.03–0.29 wt%), with F/Cl increasing from about 2 to 27. Barium is enriched, up to 9.02 wt% BaO, a typical feature of micas from lamprophyre–carbonatite complexes (Seifert *et al*.

2000), but does not contain Sr and Rb at detectable levels.

Apatite is a major repository of chlorine (0.13 to 2.91 wt% Cl), but it is extremely depleted in F, as is found in apatite in carbonatite-metasomatized mantle lherzolites (O'Reilly & Griffin 2000). However, the Finero apatite is poor in Th and U, as these elements were incorporated in specific Th–U phases. Apatite also carries the light REE (La, Ce, Pr, Nd) at concentrations between 0.08 and 0.33 wt% oxide, with Ce predominant over the other REE.

Finally, the composition of the Finero zirconolite, characterized by high Th and U contents, shows similarity with zirconolite from some carbonatite complexes, characterized by the prevalence of Th and U over Nb and Ta. Zirconolite and the associated Zr–Th–U minerals carry carbonatite-compatible elements such as Y, Hf, and Pb, and are major concentrators of the LREE. They account for the enrichment of La, Ce, and Nd observed in the chromitites with respect to the groundmass peridotites (Garuti *et al*. 2001, Grieco *et al*. 2001). These mineralogical features are symptomatic of the presence of an alkaline fluid phase with a carbonatitic signature in the chromitites of Finero.

It has recently been proposed that an alkaline-carbonatite type of fluid may have originated in the Finero mantle by immiscibility-induced segregation from an initially homogeneous SiO_2–H_2O agent rich in incompatible elements, and may have reacted heterogeneously with the mantle protolith, producing the apatite–carbonate metasomatic banding at a mesoscopic scale (Zanetti *et al*. 1999, Morishita *et al*. 2003). There is no evidence for such a segregation process nor for a two-step metasomatism with a different geochemical signature in the Finero chromitites (Grieco *et al*. 2001).

The sharp drop in T and $f(O_2)$, inferred for the crystallization of zirconolite and the formation of the symplectite assemblage, represents the last stage of the metasomatism, in which the activity of volatile components (Cl, P, CO_2) reached a maximum, causing the observed reaction between chromian spinel and olivine. However, the occurrence of metasomatic minerals (carbonates, zircon, thorianite, uraninite, baddeleyite and thorite or huttonite) in high-temperature chromite–silicate assemblages, independent of the symplectite reaction-zones, indicates that the alkaline-carbonatite signature was a primary feature of the metasomatic fluid in the Finero chromitites. The alkaline-carbonatite fluid phase may have been generated by liquid immiscibility, possibly at the core of the mantle body of Finero, and migrated outward to the marginal zones. The fact that the chromitites are concentrated at the periphery of the mantle body and display a clear enrichment in several carbonatite-compatible elements (the LREE, Zr, Th, U, Hf, Y, Pb) with respect to the average composition of the phlogopite peridotite of Finero suggests that the chromitites formed as a result of the alkaline metasomatic process.

CONCLUSIONS

(1) The small podiform bodies of chromitite in the marginal zones of the phlogopite peridotite of Finero formed by reaction of a clinopyroxene-poor, Cr-rich harzburgitic protholith with an alkaline-carbonatite fluid.

(2) This fluid may have formed from an original melt composed of undetermined proportions of a carbonatite end-member and a hydrous silicate end member. The composition of this parental melt was inferred from the observed assemblages of metasomatic minerals. It suggests the presence of a H_2O–CO_2-rich peridotite source in the mantle section below the region of emplacement of the Finero phlogopite peridotite.

(3) The formation of carbonatite-rich liquids and hydrous fluids is a common phenomenon linked to the emplacement of mantle plumes in continental rift systems worldwide. Our finding supports the concept of metasomatism of the Finero mantle as a result of mantle uplifting at the base of the continental crust. This uplift again was induced by local transtensional opening in pre-Hercynian times (Ernst 1981, Exley *et al.* 1982, Shervais & Mukasa 1991).

(4) Metasomatism produced positive anomalies in many incompatible elements in the phlogopite peridotite of Finero with respect to primitive mantle; Th and U, however, are depleted (Lu *et al.* 1997, Garuti *et al.* 2001). Our discovery of thorianite, thorite, uraninite, Th–U-rich zirconolite and baddeleyite associated with the chromitites suggests that both Th and U were important components of the carbonatitic fluid. However, these elements were not detected in the peridotites, being preferentially concentrated in the chromitite-form-

ing system. We suggest that the metasomatic event at Finero is genetically related to the intrusion of Th–U-rich alkaline-ultramafic pipes, the magmatic episode that marks the closure of the underplating event in the Ivrea Zone at about 287 ± 3 Ma (Garuti *et al.* 2001).

REFERENCES

BALLHAUS, C. BERRY, R.F. & GREEN, D.H. (1991): High pressure experimental calibration on the olivine – orthopyroxene – spinel oxygen geobarometer: implications for the oxidation state of the upper mantle. *Contrib. Mineral. Petrol.* **107**, 27-40.

BAYLISS, P., MAZZI, F., MUNNO, R. & WHITE, T.J. (1989): Mineral nomenclature: zirconolite. *Mineral. Mag.* **53**, 565-569.

BELLATRECCIA, F., DELLA VENTURA, G., CAPRILLI, E., WILLIAMS, C.T. & PARODI, G.C. (1999): Crystal-chemistry of zirconolite and calzirtite from Jacupiranga, Saõ Paulo (Brazil). *Mineral. Mag.* **63**, 649-660.

BULAKH, A.G., NESTEROV, A.R., ANASTASENKO, G.F. & ANISIMOV, I.S. (1999): Crystal morphology and intergrowths of calzirtite $Ca_2Zr_5Ti_2O_{16}$, zirkelite (Ti,Ca,Zr)O_{2-x}, zirconolite $CaZrTi_2O_7$ in phoscorites and carbonatites of the Kola Peninsula (Russia). *Neues Jahrb. Mineral., Monatsh.*, 11-20.

_____, _____, WILLIAMS, C.T. & ASIMOV, I.S. (1998): Zirkelite from the Sebl'yavr carbonatite complex, Kola Peninsula, Russia: an X-ray and electron microprobe study of a partially metamict mineral. *Mineral. Mag.* **62**, 837-846.

BUSCHE, F.D., PRINZ, M., KEIL, K. & KURAT, G. (1972): Lunar zirkelite a uranium-bearing phase. *Earth Planet. Sci. Lett.* **14**, 313-321.

CARLIER, G. & LORAND, J.-P. (2003): Petrogenesis of a zirconolite-bearing Mediterranean-type lamproite from the Peruvian Altiplano (Andean Cordillera). *Lithos* **69**, 15-35.

CAWTHORN, R.G. (1975): The amphibole peridotite–metagabbro complex, Finero, northern Italy. *J. Geol.* **83**, 437-454.

COLTORTI, M. & SIENA, F. (1984): Mantle tectonite and fractionate peridotite at Finero (Italian Western Alps). *Neues Jahrb. Mineral., Abh.* **149**, 225-244.

CUMMINGS, G.L., KÖPPEL, V. & FERRARIO A. (1987): A lead isotope study of the northeastern Ivrea Zone and the adjoining Ceneri zone (N. Italy): evidence for a contaminated subcontinental mantle. *Contrib. Mineral. Petrol.* **97**, 19-30.

DAWSON, J.B. & SMITH, J.V. (1977): The MARID (mica – amphibole – rutile – ilmenite – diopside) suite of xenoliths in kimberlite. *Geochim. Cosmochim. Acta* **41**, 309-323.

DE HOOG, J.C.M. & VAN BERGEN, M.J. (2000): Volatile-induced transport of HFSE, REE, Th and U in arc magmas: evidence from zirconolite-bearing vesicles in potassic lavas of Lewotolo volcano (Indonesia). *Contrib. Mineral. Petrol.* **139**, 485-502.

DELLA VENTURA, G., BELLATRECCIA, F. & WILLIAMS, C.T. (2000): Zirconolite with significant REEZrNb(Mn,Fe)O$_7$ from a xenolith of the Laacher See eruptive center, Eifel volcanic region, Germany). *Can. Mineral.* **38**, 57-65.

DONOVAN, J.J. & RIVERS, M.L. (1990): PRSUPR – a PC based automation and analyses software package for wavelength dispersive electron beam microanalysis. *Microbeam Anal.*, 66-68.

ERLANK, A.J., WATERS, F.G., HAWKESWORTH, C.J., HAGGERTY, S.E., ALLSOPP, H.L., RICKARD, R.S. & MENZIES, M.A. (1987): Evidence for mantle metasomatism in peridotite nodules from the Kimberley pipes, South Africa. *In* Mantle Metasomatism (M.A. Menzies & C.J.Hawkesworth, eds.). Academic Press, London, U.K. (221-311).

ERNST, W.G. (1978): Petrochemical study of lherzolite rocks from the Western Alps. *J. Petrol.* **19**, 341-392.

_____ (1981): Petrogenesis of eclogites and peridotites from the Western and Ligurian Alps. *Am. Mineral.* **66**, 443-472.

EXLEY, R.A., SILLS, J.D. & SMITH, J.V. (1982): Geochemistry of micas from the Finero spinel-lherzolite, Italian Alps. *Contrib. Mineral. Petrol.* **81**, 59-63.

FERRARIO, A. & GARUTI, G. (1990): Platinum-group mineral inclusions in chromitites of the Finero mafic–ultramafic complex (Ivrea-Zone, Italy). *Mineral. Petrol.* **41**, 125-143.

FOWLER, M. & WILLIAMS, C.T. (1986): Zirconolite from the Glen Dessarry syenite: a comparison with other Scottish localities. *Mineral. Mag.* **50**, 326-328.

GARUTI, G., BEA, F., ZACCARINI, F. & MONTERO, P. (2001): Age, geochemistry, and petrogenesis of the ultramafic pipes of the Ivrea Zone, NW Italy. *J. Petrol.* **42**, 433-457.

_____ & FRIOLO, F. (1978): Textural features and olivine fabrics of peridotites from the Ivrea–Verbano Zone (Italian Western Alps). *Mem. Sci. Geol.* **XXXIII**, 111-125.

_____, ODDONE, M. & TORRES R.J. (1997): Platinum-group-element distribution in subcontinental mantle: evidence from the Ivrea Zone (Italy) and the Betic–Rifean Cordillera (Spain and Morocco). *Can. J. Earth Sci.* **34**, 444-463.

GIERÉ, R. (1986): Zirconolite, allanite, and hoegbomite in a marble skarn from the Bergell contact aureole: implication for mobility of Ti, Zr and REE). *Contrib. Mineral. Petrol.* **93**, 459-470.

_____ (1990): Hydrothermal mobility of Ti, Zr and REE: examples from the Bergell and Adamello contact aureoles (Italy). *Terra Nova* **2**, 60-67.

_____ & WILLIAMS, C.T. (1992): REE-bearing minerals in a Ti-rich vein from the Adamello contact aureole (Italy). *Contrib. Mineral. Petrol.* **112**, 83-100.

_____, _____ & LUMPKIN, G.R. (1998): Chemical characteristic of natural zirconolite. *Schweiz. Mineral. Petrogr. Mitt.* **78**, 433-459.

GRIECO, G., FERRARIO, A., VON QUADT, A., KOEPPEL, V. & MATHEZ, E.A. (2001): The zircon-bearing chromitites of the phlogopite peridotite of Finero (Ivrea Zone, Southern Alps): evidence and geochronology of a metasomatized mantle slab. *J. Petrol.* **42**, 89-101.

HAGGERTY, S.E. (1987): Metasomatic mineral titanates in upper mantle xenoliths. *In* Mantle Xenoliths (P.H. Nixon, ed.). Clarendon Press, Oxford, U.K. (87-109).

_____ (1995): Upper mantle mineralogy. *J. Geodyn.* **20**, 331-364.

HARDING, R.R., MERRIMAN, R.J. & NANCARROW, P.H.A. (1982): A note on the occurrence of chevkinite, allanite and zirkelite on St. Kilda, Scotland. *Mineral. Mag.* **46**, 445-448.

HARLEY, S.L. (1994): Mg–Al yttrian zirconolite in a partially melted sapphirine granulite, Vestfold Hills, East Antarctica. *Mineral. Mag.* **58**, 259-269.

HARTE, B., WINTERBURN, P.A. & GURNEY, J.J. (1987): Metasomatic and enrichment phenomena in garnet peridotite facies mantle xenoliths from the Matsoku kimberlite pipe, Lesotho. *In* Mantle Metasomatism (M.A. Menzies & C.J. Hawkesworth, eds.). Academic Press, London, U.K. (145- 220).

HARTMANN, G. & WEDEPOHL, K. H. (1993): The composition of peridotites tectonites from the Ivrea Complex, northern Italy: residues from melt extraction. *Geochim. Cosmochim. Acta* **57**, 1761-1782.

HENK, A., FRANZ, L., TEUFEL, S. & ONCKEN, O. (1997): Magmatic underplating extension, and crustal reequilibration: insights from a cross-section through the Ivrea Zone and Strona-Ceneri Zone, northern Italy. *J. Geol.* **105**, 367-377.

HORNING, I. & WÖRNER, G. (1991): Zirconolite-bearing ultrapotassic veins in a mantle xenolith from Mt. Melbourne Volcanic Field, Victoria Land, Antarctica. *Contrib. Mineral. Petrol.* **106**, 355-366.

HUNZIKER, J.K. (1974): Rb–Sr and K–Ar age determination and Alpine tectonic history of the Western Alps. *Ist. Geol. Mineral. Univ. Padova, Mem.* **31**, 1-54.

LENSCH, G. (1968): Die Ultramafite der Zone von Ivrea und ihre geologishe Interpretation. *Scwheiz. Mineral. Petrogr. Mitt.* **48**, 91-102.

LORAND, J.-P. & COTTIN, J.Y. (1987): A new natural occurrence of zirconolite ($CaZrTi_2O_7$) and baddeleyite (ZrO_2) in basic cumulates: the Laouni layered intrusion (southern Hoggar, Algeria). *Mineral. Mag.* **51**, 671-676.

LU, MEIHUA, HOFMANN, A.W., MAZZUCCHELLI, M. & RIVALENTI, G. (1997): The mafic–ultramafic complex near Finero (Ivrea–Verbano Zone). 1. Chemistry of MORB-like magmas. *Chem. Geol.* **140**, 207-222.

MAZZI, F. & MUNNO, R. (1983): Calciobetafite (new mineral of the pyrochlore group) and related minerals from Campi Flegrei, Italy; crystal structure of polymignyte and zirkelite: comparison with pyrochlore and zirconolite). *Am. Mineral.* **68**, 262-276.

MORISHITA, T., ARAI, S. & TAMURA, A. (2003): Petrology of an apatite-rich layer in the Finero phlogopite-peridotite, Italian Western Alps: implications for evolution of a metasomatising agent. *Lithos* **69**, 37-49.

O'REILLY, S. & GRIFFIN, W.L. (2000): Apatite in the mantle: implication for metasomatic processes and high heat production in Phanerozoic mantle. *Lithos* **53**, 217-232.

PLATT, G., WALL, F., WILLIAMS, C.T. & WOOLLEY, A.R. (1987): Zirconolite, chevkinite and other rare earth minerals from nepheline syenites and peralkaline granites and syenites of the Chilwa alkaline province, Malawi. *Mineral. Mag.* **51**, 253-263.

PROENZA, J.A., MELGAREJO, J.C., GERVILLA, F. & LLOVET, X. (2001): Y-zirconolita en cromititas ofioliticas de Cuba oriental. Implicaciones petrogeneticas. *Bol. Soc. Esp. Mineral.* **24A**, 39-40 (abstr.).

PURTSCHELLER, F. & TESSADRI, R. (1985): Zirconolite and baddeleyite from metacarbonates of the Oetztal–Stubai complex (northern Tyrol, Austria). *Mineral. Mag.* **49**, 523-529.

SEIFERT, W., KÄMPF, H. & WASTERNACK, J. (2000): Compositional variation in apatite, phlogopite and other accessory minerals of the ultramafic Delitzsch complex, Germany: implication for cooling history of carbonatites. *Lithos* **53**, 81-100.

SHENG, Y.J., HUTCHEON, I.D. & WASSERBURG, G.J. (1991): Origin of plagioclase–olivine inclusions in carbonaceous chondrites. *Geochim. Cosmochim. Acta* **55**, 581-599.

SHERVAIS, J.W. & MUKASA, S.B. (1991): The Balmuccia orogenic lherzolite massif, Italy. *J. Petrol., Lherzolite Special Issue*, 155-174.

SONNENTHAL, E.L. (1992): Geochemistry of dendritic anorthosites and associated pegmatites in Skaergaard Intrusion, East Greenland: evidence for metasomatism by a chlorine-rich fluid. *J. Volcan. Geotherm. Res.* **52**, 209-230.

STÄHLE, V., FRENZEL, G., KOBER, B., MICHARD, A., PUCHELT, H. & SCHNEIDER, W. (1990): Zircon syenite pegmatites in the Finero peridotite (Ivrea zone): evidence for a syenite from a mantle source. *Earth Planet. Sci. Lett.* **101**, 196-205.

STUCKI, A, TROMMSDORFF, V. & GUNTHER, D. (2001): Zirconolite in metarodingites of Penninic Mesozoic ophiolites, Central Alps. *Schweiz. Mineral. Petrogr. Mitt.* **81**, 257-265.

VON QUADT, A., FERRARIO, A., DIELLA, V., HANSMANN, W., VAVRA, G. & KÖPPEL, V. (1993): Zircon U–Pb ages from chromitites of the phlogopite peridotite of Finero, Ivrea zone, N-Italy. *Terra abstract* **5**, 393-394.

VOSHAGE, H., HUNZIKER, J.C., HOFMANN, A.W. & ZINGG, A. (1987): A Nd and Sr isotopic study of the Ivrea zone, Southern Alps, N Italy. *Contrib. Mineral. Petrol.* **97**, 31-42.

WILLIAMS, C.T. (1978): Uranium-enrichment minerals in mesostasis areas of the Rhum layered pluton. *Contrib. Mineral. Petrol.* **66**, 29-39.

_____ & GIERÉ, R. (1996): Zirconolite: a review of localities worldwide, and a compilation of its chemical compositions. *Bull. Nat. Hist. Mus. Lond.* (*Geol.*) **52**, 1-24.

ZAKRZEWSKI, M.A., LUSTENHOUWER, W.J., NUGTEREN, H.J. & WILLIAMS, C.T. (1992): Rare-earth minerals yttrian zirconolite and allanite-(Ce) and associated minerals from Koberg mine, Bergslagen, Sweden. *Mineral. Mag.* **56**, 27-35.

ZANETTI, A., MAZZUCCHELLI, M., RIVALENTI, G. & VANNUCCI, R. (1999): The Finero phlogopite-peridotite massif: an example of subduction-related metasomatism. *Contrib. Mineral. Petrol.* **134**, 107-122.